

## Supplementary Information File for

### Structural basis and molecular mechanism of biased GPBAR signalling in regulating NSCLC cell growth via YAP activity

Lijuan Ma<sup>a,b,1</sup>, Fan Yang<sup>a,b,c,d,1</sup>, Xiang Wu<sup>a,b,1</sup>, Chunyou Mao<sup>e,1</sup>, Lulu Guo<sup>a,b</sup>, Tianshu Miao<sup>a,b</sup>, Shao-Kun Zang<sup>f, g, h, i</sup>, Xiaoyu Jiang<sup>a,b</sup>, Dan-Dan Shen<sup>f, g, h, i</sup>, Tianhui Wei<sup>j</sup>, Hengxing Zhou<sup>j, k</sup>, Qin Wei<sup>a,b</sup>, Shiyang Li<sup>d</sup>, Qiang Shu<sup>j, m</sup>, Shiqing Feng<sup>j, k</sup>, Changtao Jiang<sup>l</sup>, Bo Chu<sup>a,b</sup>, Luta Du<sup>n,\*</sup>, Jin-Peng Sun<sup>a,b, d, l,\*</sup>, Xiao Yu<sup>b,c,\*</sup>, Yan Zhang<sup>e,f, g, h, i,\*</sup>, Pengju Zhang<sup>a,b,\*</sup>

#### Affiliations:

<sup>a</sup> Department of Biochemistry and Molecular Biology, School of Basic Medical Sciences, Cheeloo College of Medicine, Shandong University, Jinan, Shandong 250012, China.

<sup>b</sup> Key Laboratory Experimental Teratology of the Ministry of Education, Shandong University, Jinan, Shandong, 250012, China.

<sup>c</sup> Department of Physiology, School of Basic Medical Sciences, Shandong University, Jinan, Shandong 250012, China.

<sup>d</sup> Advanced Medical Research Institute, Shandong University, Jinan, Shandong, 250012, China.

<sup>e</sup> Center for Structural Pharmacology and Therapeutics Development, Sir Run Run Shaw Hospital, Zhejiang University School of Medicine, Hangzhou, Zhejiang, 310058, China;

<sup>f</sup> Department of Biophysics and Department of Pathology of Sir Run Run Shaw Hospital, Zhejiang University School of Medicine, Hangzhou, Zhejiang, 310058, China.

<sup>g</sup> Liangzhu Laboratory, Zhejiang University Medical Center, Hangzhou, 310058, China.

<sup>h</sup> MOE Frontier Science Center for Brain Research and Brain-Machine Integration, Zhejiang University School of Medicine, Hangzhou, Zhejiang, 310058, China.

<sup>i</sup> Zhejiang Province Key Laboratory of Immunity and Inflammatory Diseases, Hangzhou, 310058, Zhejiang, China.

<sup>j</sup> Qilu Hospital, Cheeloo College of Medicine, Shandong University, Jinan, 250012, China.

<sup>k</sup> Center for Orthopaedics, Cheeloo College of Medicine, Shandong University, Jinan, 250012, China.

<sup>l</sup> Key Laboratory of Molecular Cardiovascular Science, Ministry of Education, Department of Physiology and Pathophysiology, School of Basic Medical Sciences, Peking University, Beijing, 100191, China.

<sup>m</sup> Shandong Provincial Clinical Research Center for Immune Diseases and Gout, Jinan, Shandong, 250033, China

<sup>n</sup> Department of Clinical Laboratory, The Second Hospital of Shandong University, Jinan, 250033, China.

<sup>1</sup> L.J.M., F.Y., X.W., and C.Y.M. contributed equally to this work.

\*Corresponding author. Email: [lutaodu@sdu.edu.cn](mailto:lutaodu@sdu.edu.cn);  
[sunjinpeng@sdu.edu.cn](mailto:sunjinpeng@sdu.edu.cn) ;  
[zhang\\_yan@zju.edu.cn](mailto:zhang_yan@zju.edu.cn);  
[yuxiao@sdu.edu.cn](mailto:yuxiao@sdu.edu.cn);  
[zhpj@sdu.edu.cn](mailto:zhpj@sdu.edu.cn)

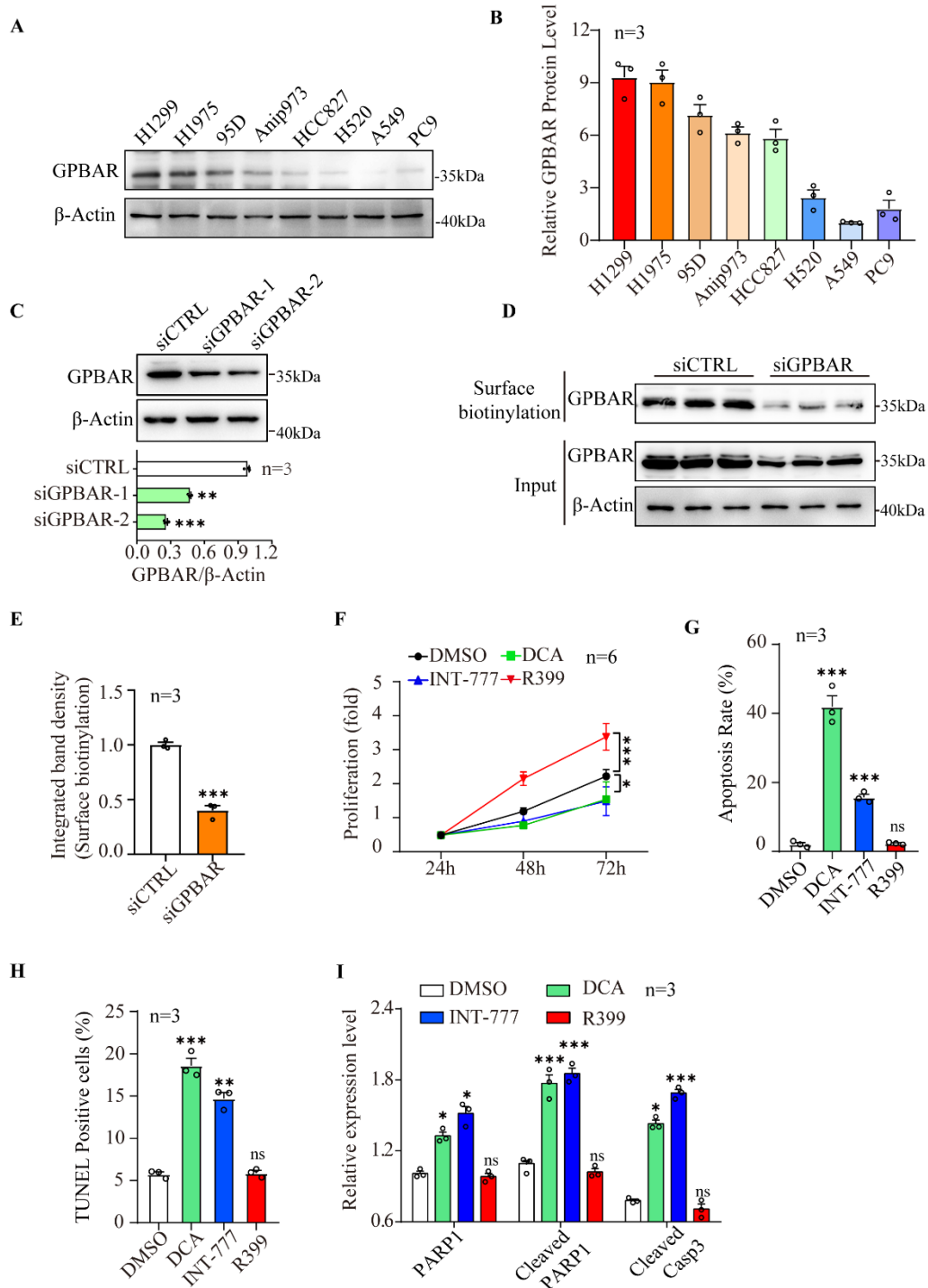
**This Supplementary Information File includes:**

Supplemental Figures 1-20

Supplemental Tables 1-7

Supplemental Methods and Materials

## Supplementary Figures



**Supplementary Fig. 1 R399 enhances cell growth while INT-777 inhibits cell growth in H1299 cells.**

**(A)** GPBAR protein expression in different types of NSCLC cell lines were evaluated by western blot.

**(B)** Quantitative analyses were shown in the graphs (n=3). Data are normalized according to the expression in A549 cells.

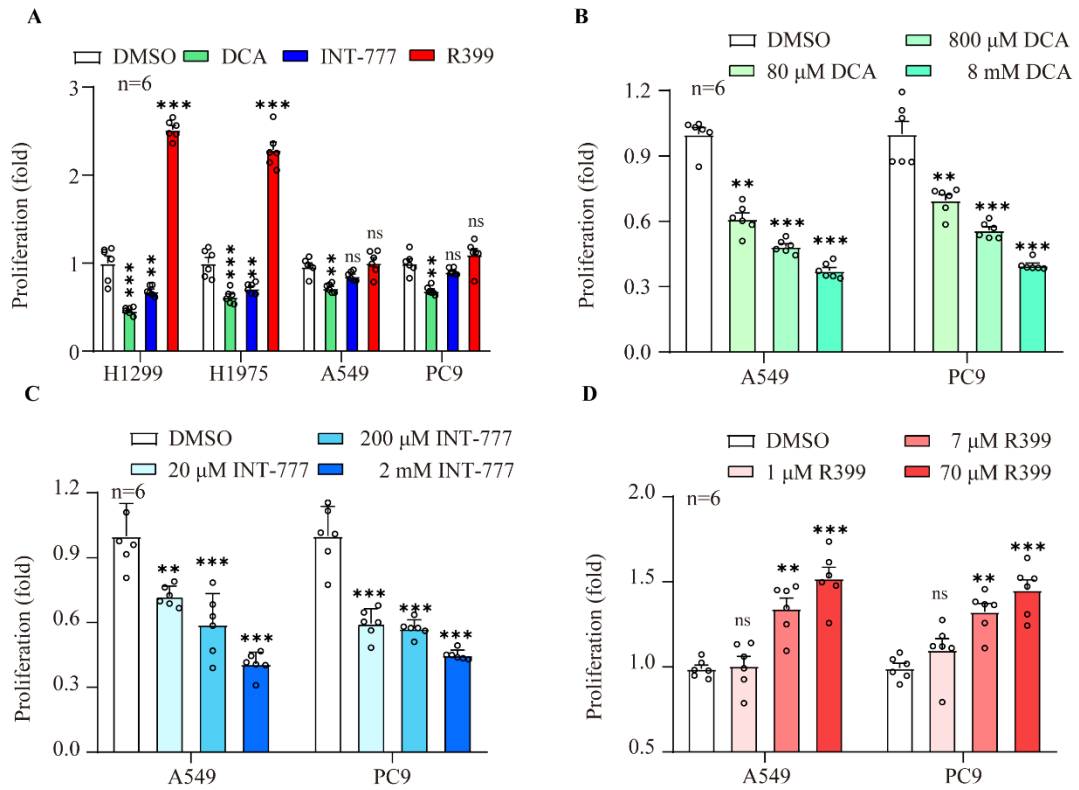
**(C)** GPBAR was depleted by specific siRNAs in H1299 cells as indicated. The protein of GPBAR was analyzed by western blot, with  $\beta$ -Actin as a loading control. Quantitative analyses were shown in the graphs (n=3).

**(D-E)** Surface biotinylation assay to evaluate the cell surface expression levels of GPBAR transfected with siGPBAR or siCTRL in H1299 cells **(D)**. Quantitative analyses were shown in the graph (n=3) **(E)**.

**(F)** H1299 cells were treated with DMSO, DCA (80  $\mu$ M), INT-777 (2  $\mu$ M) and R399 (700 nM) for the indicated time, respectively. The cell viability was assessed using MTT assay (n=6).

**(G-I)** Following the same settings as in **(F)**, the apoptotic rates of cells were detected by flow cytometry analysis (n=3) **(G)**. Quantitative analyses of the TUNEL-positive cell ratio were shown in the graphs (n=3) **(H)**. Quantitative analyses of PARP1, cleaved PARP1 and cleaved caspase-3 detected by western blot in H1299 cells **(I)**.

All data are presented by mean  $\pm$ SEM. ns: not significant, \*P<0.05, \*\*P<0.01, \*\*\*P<0.001 based on the Student's t-test. All results are representative of three independent experiments.

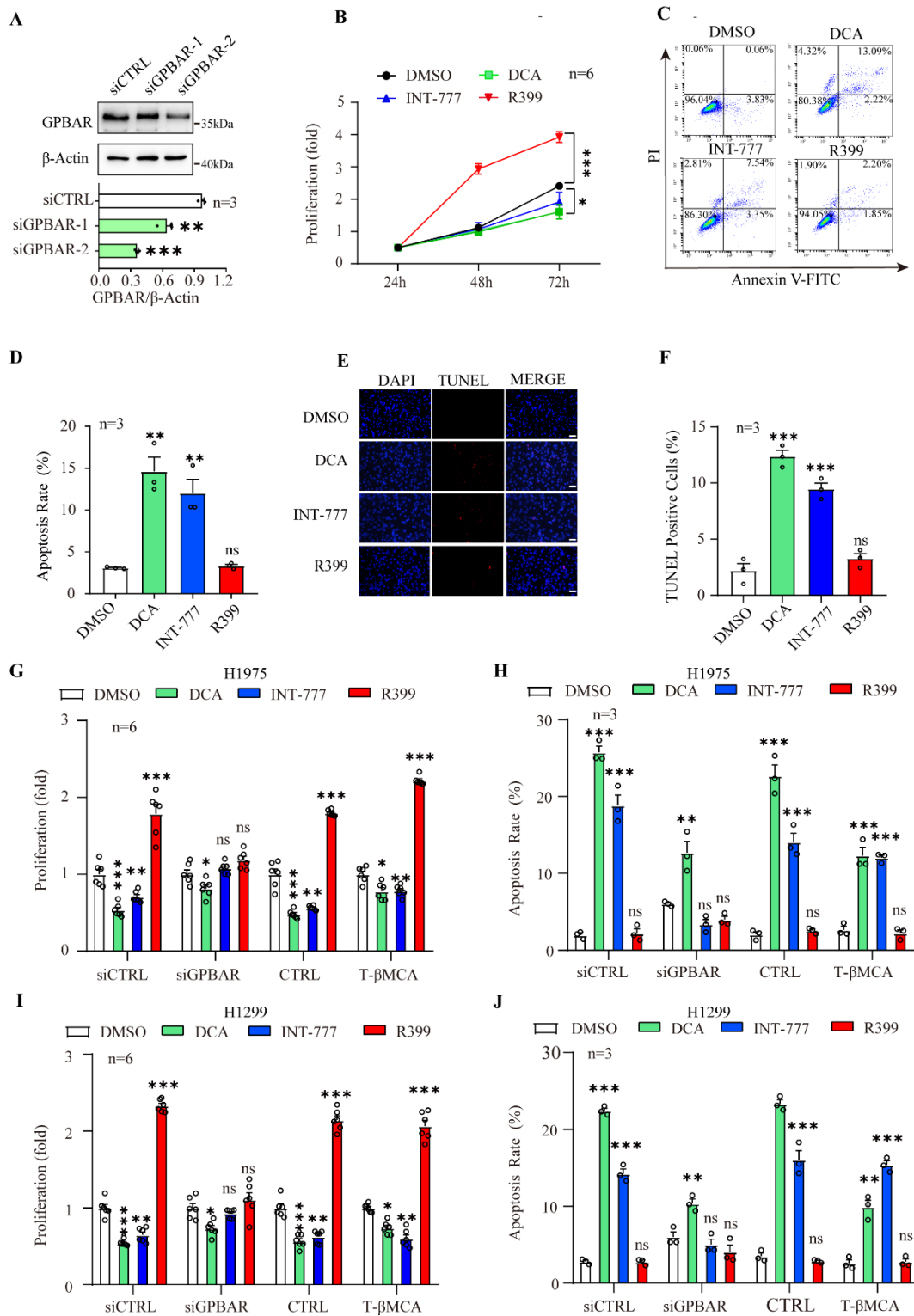


**Supplementary Fig. 2 R399 promotes cell growth but INT-777 inhibits cell growth in NSCLC cells.**

**(A)** H1299, H1975, A549 and PC9 cells were treated with DMSO, DCA (80  $\mu$ M), INT-777 (2  $\mu$ M) and R399 (700 nM) for 72 h respectively. The cell viability was assessed using MTT assay (n=6).

**(B-D)** A549 and PC9 cells were treated with DMSO, DCA (80  $\mu$ M, 800  $\mu$ M, 8 mM) **(B)**, INT-777 (20  $\mu$ M, 200  $\mu$ M, 2mM) **(C)** and R399 (1  $\mu$ M, 7  $\mu$ M, 70  $\mu$ M) **(D)** for 72 h respectively. The cell viability was assessed using MTT assay (n=6).

All data are presented by mean  $\pm$  SEM. ns: not significant, \*\*P<0.01, \*\*\*P<0.001 based on the Student's t-test.



**Supplementary Fig. 3 R399 promotes cell growth but INT-777 inhibits cell growth GPBAR-dependently in H1975 and H1299 cells.**

**(A)** GPBAR was depleted by specific siRNAs in H1975 cells as indicated. GPBAR protein was analyzed by western blot, with  $\beta$ -Actin as a loading control. Quantitative analyses were shown in the graphs (n=3).

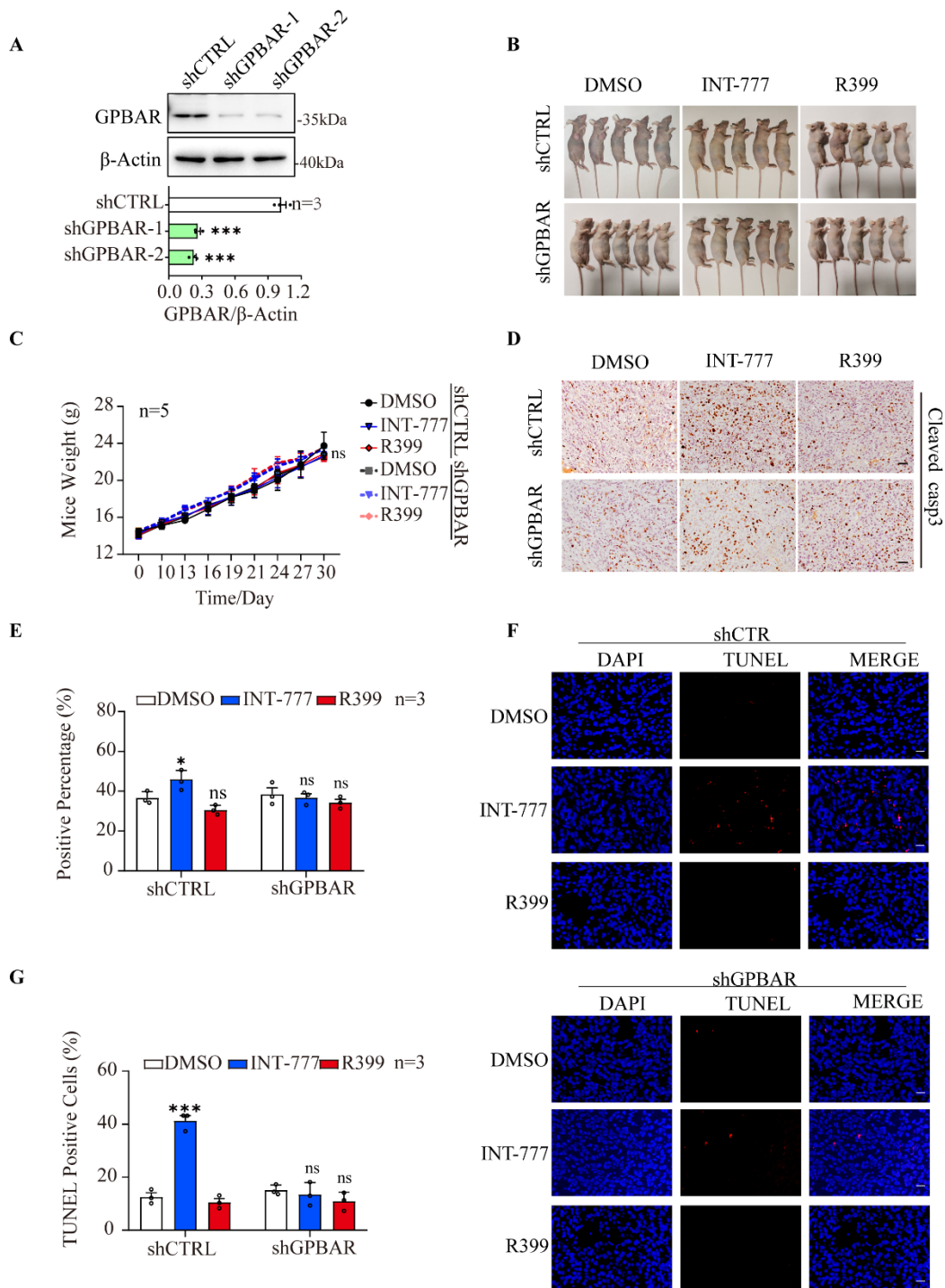
**(B)** H1975 cells were treated with DMSO, DCA (80  $\mu$ M), INT-777 (2  $\mu$ M) and R399 (700 nM) for 24 h, 48 h and 72 h, respectively. The cell viability was assessed using MTT assay (n=6).

**(C-F)** H1975 cells were treated with DMSO, DCA (80  $\mu$ M), INT-777 (2  $\mu$ M) and R399 (700 nM) for 24 h respectively. The apoptotic cells were detected by flow cytometry analysis **(C)** and TUNEL staining **(E)**. Quantitative analyses were shown in the graphs **(D and F)** (n=3). The scale bars represent 50  $\mu$ m.

**(G-H)** H1975 cells transfected with scramble siRNA (siCTRL), GPBAR specific siRNAs (siGPBAR-2) and FXR inhibitor (T- $\beta$ MCA, 10  $\mu$ M) were treated with DMSO, DCA (80  $\mu$ M), INT-777 (2  $\mu$ M) and R399 (700 nM), respectively. The cell viability was assessed using MTT assay **(G)** and the cell apoptosis was examined by flow cytometry analysis **(H)**.

**(I-J)** H1299 cells transfected with scramble siRNA (siCTRL), siGPBAR-2 and FXR inhibitor (T- $\beta$ MCA, 10  $\mu$ M) were treated with DMSO, DCA (80  $\mu$ M), INT-777 (2  $\mu$ M) and R399 (700 nM), respectively. The cell viability was assessed using MTT assay **(I)** and the cell apoptosis was examined by flow cytometry analysis **(J)**.

All data are presented by mean  $\pm$ SEM. ns: not significant, \*P<0.05, \*\*P<0.01, \*\*\*P<0.001 based on the Student's t-test. All results are representative of three independent experiments.



**Supplementary Fig. 4 R399 promotes but INT-777 inhibits tumorigenesis *in vivo* in a GPBAR-dependent manner.**

(A) GPBAR was depleted by specific shRNAs in H1299 cells as indicated. The protein of GPBAR was analyzed by western blot, with  $\beta$ -Actin as a loading control. Quantitative analyses were shown in the graphs (n=3).

(B) The photographs of different group of nude mice.



(C) Quantification of body weights of mice with different treatment were calculated.

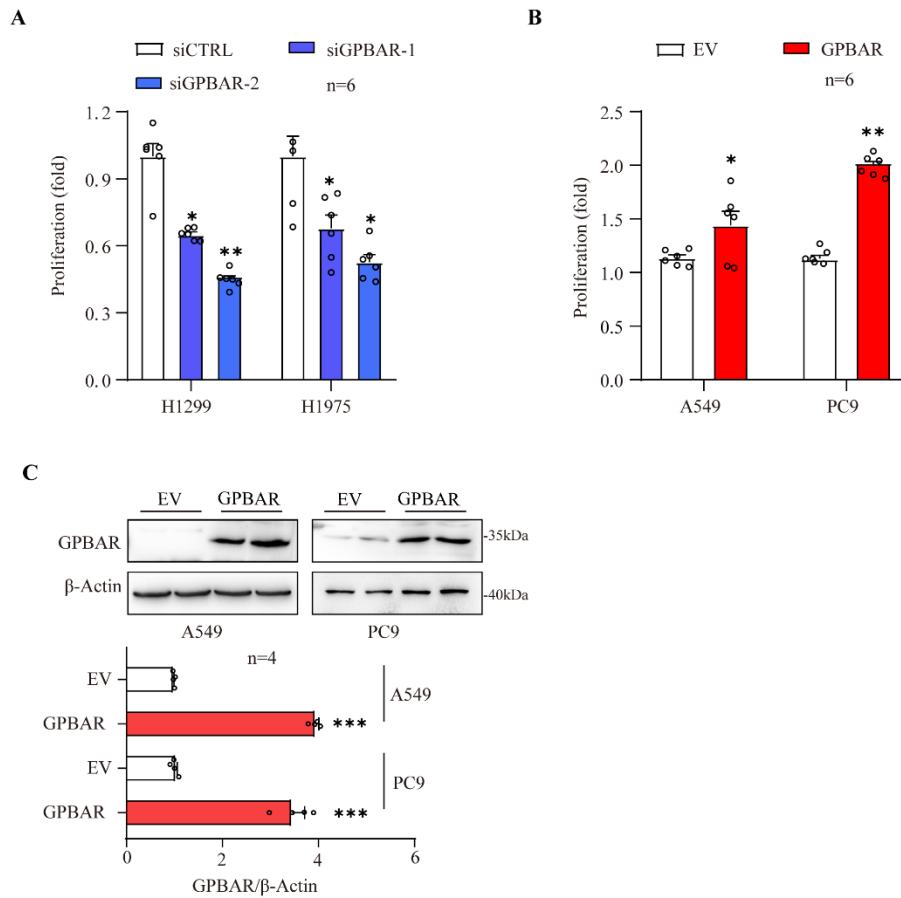
(D-E) Cell apoptosis was detected by Cleaved Caspase3 staining of the tumor sections

(D) Quantitative analyses of the percentage of Cleaved Caspase3 positive cells were shown in the graphs (n=3) (E). The scale bars represent 50  $\mu\text{m}$ .

(F) Cell apoptosis was detected using TUNEL assay of the tumor sections. Nuclei were counterstained with DAPI (blue). The scale bars represent 50  $\mu\text{m}$ .

(G) Quantitative analyses of TUNEL positive cell ratio of each group (n=3).

All data are presented by mean  $\pm$ SEM. ns: not significant, \*P<0.05, \*\*P<0.01, \*\*\*P<0.001 based on the Student's t-test. All results are representative of three independent experiments.



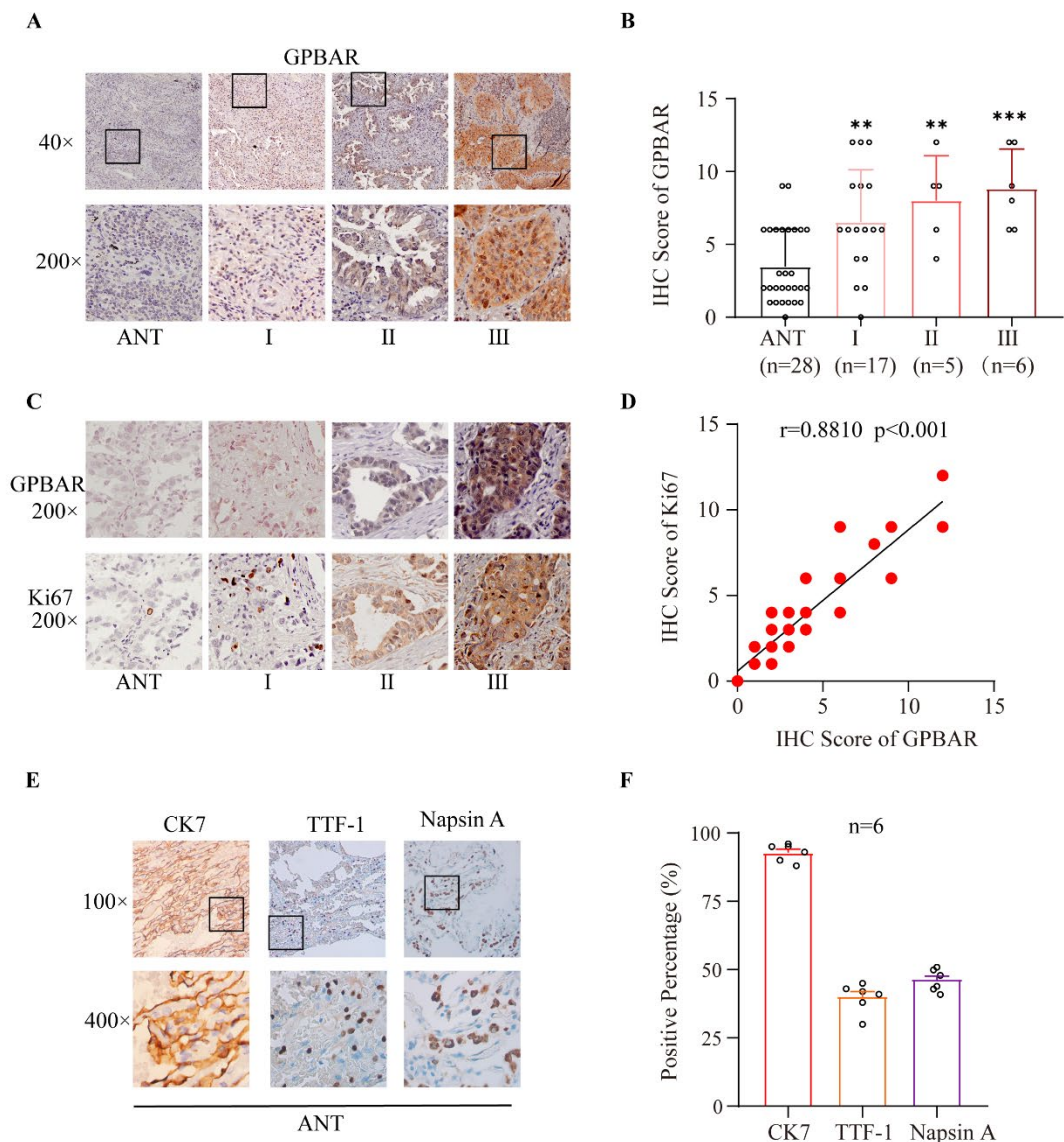
**Supplementary Fig. 5 GPBAR promotes cell growth in NSCLC cells.**

(A) MTT analysis was performed to detect the effects of GPBAR silencing on cell growth of H1299 and H1975 cells (n=6).

(B) MTT analysis was performed to detect the effects of GPBAR overexpression on cell growth of A549 and PC9 cells (n=6).

(C) The protein levels of GPBAR were analyzed by western blot in A549 cells and PC9 cells transfected with GPBAR expression plasmids. Quantitative analyses were shown in the graphs (n=4).

All data are presented by mean  $\pm$  SEM. \*P<0.05, \*\*P<0.01, \*\*\*P<0.001 based on the Student's t-test.



**Supplementary Fig. 6 GPBAR is highly expressed in NSCLC tissues.**

(A) The representative immunohistochemistry staining of GPBAR expression in 28 NSCLC tissues in different stages and 28 adjacent noncancerous tissues (ANTs).

(B) The quantitative analysis of GPBAR expression in 28 NSCLC tissues in different stages and 28 adjacent noncancerous tissues (ANTs).

(C) The representative immunohistochemistry staining of GPBAR and Ki67 in 28 NSCLC tissues in different stages and their adjacent noncancerous tissues (ANTs).

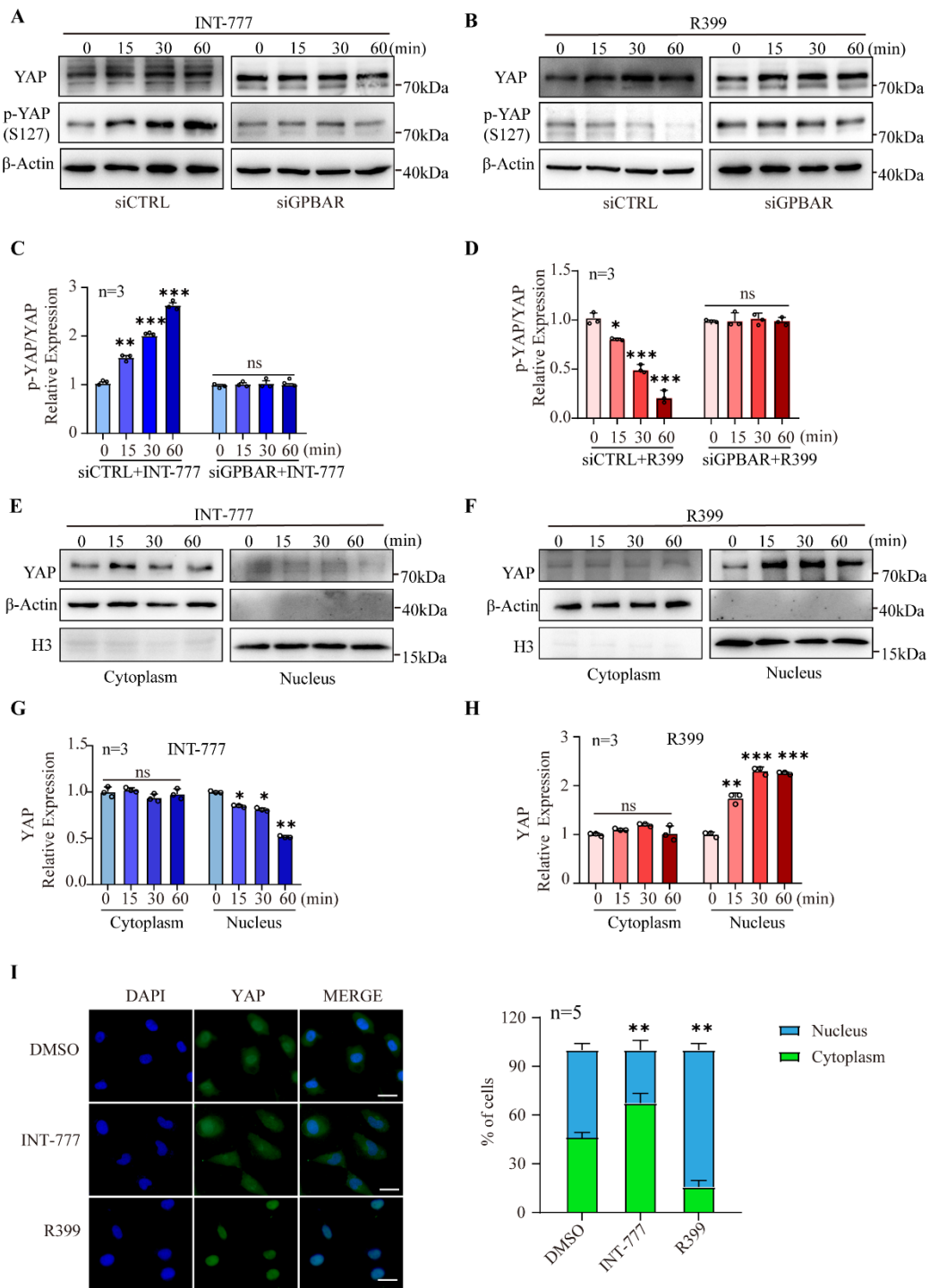
(D) The correlation between the expression of GPBAR and Ki67 in 28 NSCLC tissues in different stages and their adjacent noncancerous tissues (ANTs) (n=56).

(E) The representative immunohistochemistry staining of CK7, TTF-1 and Napsin A

in 6 adjacent noncancerous tissues (ANTs).

**(F)** Quantitative analyses of the percentage of positive cells stained with specific markers in the graphs (n=6).

All data are presented by mean  $\pm$  SEM. \*\*P<0.01, \*\*\*P<0.001 based on the Student's t-test.



**Supplementary Fig. 7 R399 and INT-777 play different roles in regulating YAP phosphorylation and nuclear shuttling.**

(A-B) Effects of INT-777 (A) and R399 (B) on YAP S127 phosphorylation were detected by western blot in H1299 cells expressing siCTRL or siGPBAR treated with INT-777 (2  $\mu$ M) or R399 (700 nM) or for the indicated time.

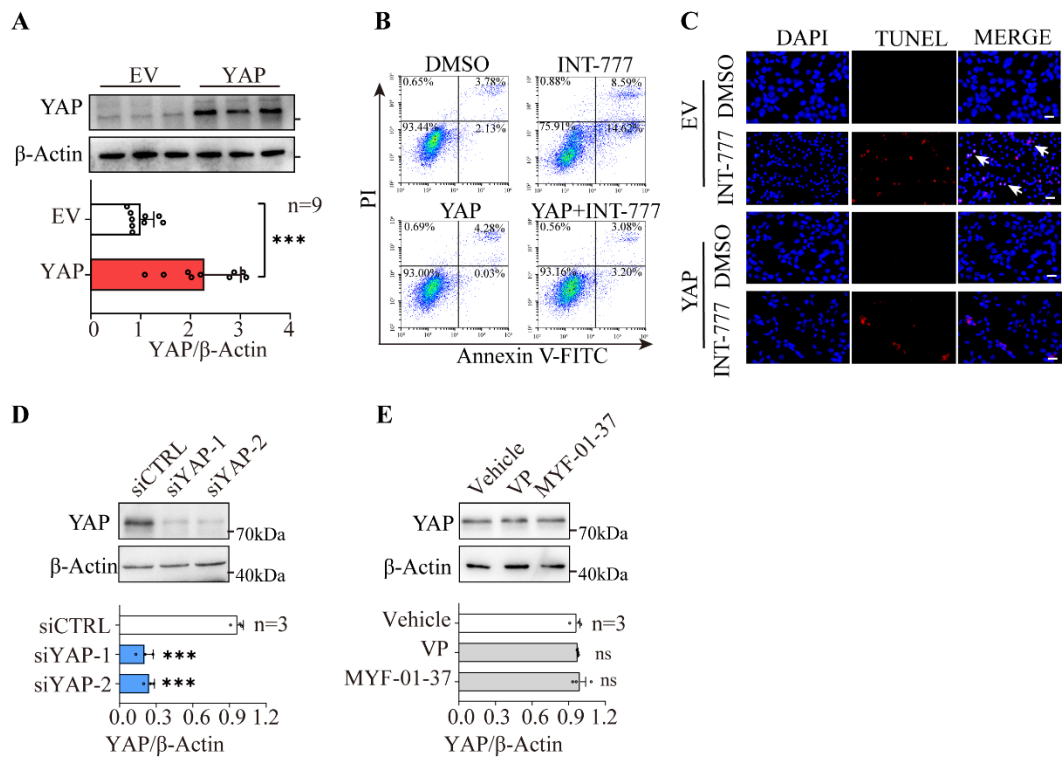
**(C-D)** Quantitative analyses of phosphor-YAP (p-YAP) detected by western blot in H1299 cells expressing siCTRL or siGPBAR treated with INT-777 (2  $\mu$ M) **(C)** or R399 (700 nM) **(D)** for the indicated time (n=3).

**(E-F)** Western blot analysis of YAP protein expression in the nuclear and cytoplasmic extracts of H1299 cells stimulated with INT-777 **(E)** (2  $\mu$ M) or R399 **(E)** (700 nM) for the indicated times.  $\beta$ -Actin and H3 were used as cytoplasmic and nuclear loading control, respectively.

**(G-H)** Quantitative analyses of YAP subcellular localization detected by western blot in H1299 cells treated with INT-777 (2  $\mu$ M) **(E)** or R399 (700 nM) **(E)** for the indicated time (n=3).

**(I)** YAP localization evaluated by immunofluorescence (IF) in H1299 cells stimulated with INT-777 (2  $\mu$ M) or R399 (700 nM). Nuclei were stained in blue (DAPI). Right graph represents the quantification of YAP nuclear vs. cytoplasmic localization. The scale bars represent 50  $\mu$ m.

All data are presented by mean $\pm$ SEM. ns: not significant, \*P<0.05, \*\*P<0.01, \*\*\*P<0.001 based on the Student's test. All results are representative of three independent experiments.



**Supplementary Fig. 8 The protein expression levels of YAP transfected with siRNAs and inhibitors.**

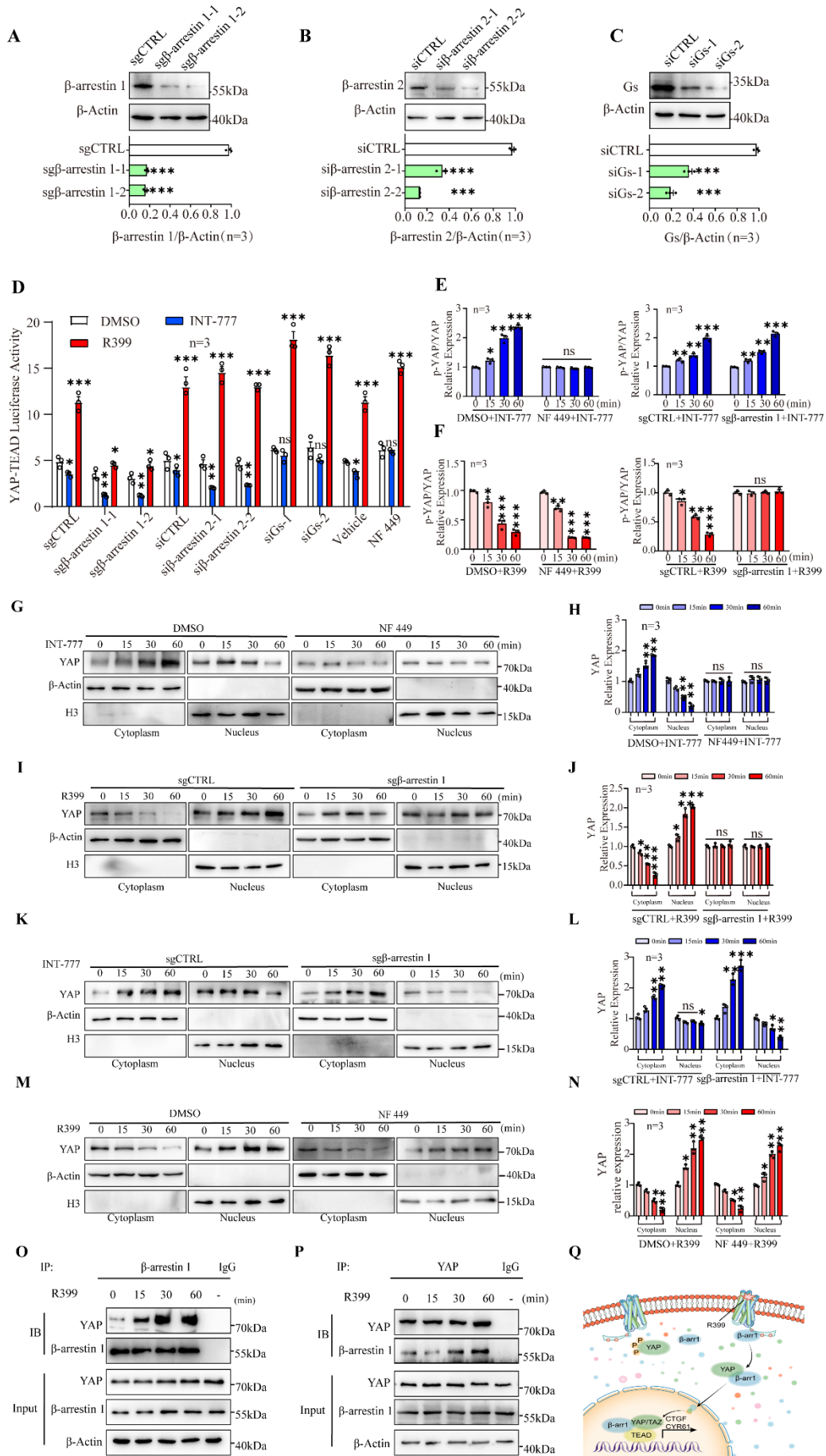
(A) The protein level of YAP was analyzed by western blot in H1299 cells transfected with YAP expression plasmids. Quantitative analyses were shown in the graph (n=9).

(B) Flow cytometry were performed to detect the effects of YAP overexpression on INT-777 (2 μM) induced cell apoptosis of H1299 cells.

(C) TUNEL analysis were performed to detect the effects of YAP overexpression on INT-777 (2 μM) induced cell apoptosis of H1299 cells. The scale bars represent 50 μm.

(D-E) The protein level of YAP was analyzed by western blot transfected with YAP specific siRNAs (D) or inhibitors (E). Quantitative analyses were shown in the graph (n=3).

All data are presented by mean±SEM. ns: not significant, \*\*\*P<0.001 based on the Student's t-test. All results are representative of three independent experiments.





**Supplementary Fig. 9 R399 and INT-777 elicit different activities of G protein and  $\beta$ -arrestin 1 to differentially control YAP activity.**

**(A)** The protein level of  $\beta$ -arrestin 1 was analyzed by western blot in H1299 cells transfected with  $\beta$ -arrestin 1 specific sgRNAs or sgCTRLs. Quantitative analyses were shown in the graph (n=3).

**(B-C)** The protein levels of  $\beta$ -arrestin 2 **(B)** and Gs **(C)** were analyzed by western blot in H1299 cells transfected with  $\beta$ -arrestin 2 specific or Gs specific siRNAs. Quantitative analyses were shown in the graphs (n=3).

**(D)** Effects of  $\beta$ -arrestin 1/2 silencing, Gs silencing or Gs inhibitor, NF 449 (10  $\mu$ M), on the changes of YAP-TEAD relative luciferase activity induced by R399 (700 nM) or INT-777 (2  $\mu$ M) (n=3).

**(E-F)** Quantitative analyses of phosphor-YAP (p-YAP) detected by western blot in H1299 cells transfected with sg $\beta$ -arrestin 1 or treated with Gs inhibitor (NF 449, 10  $\mu$ M), in combination with INT-777 (2  $\mu$ M) **(E)** or R399 (700 nM) **(F)** stimulation for the indicated time (n=3).

**(G-H)** Effects of Gs inhibitor, NF 449 (10  $\mu$ M), on the alterations of YAP subcellular localization triggered by INT-777 (2  $\mu$ M) were analyzed using western blot **(G)**. Quantitative analyses were shown in the graph (n=3) **(H)**.

**(I-J)** Effects of  $\beta$ -arrestin 1 silencing on the alterations of YAP subcellular localization triggered by R399 (700 nM) were analyzed using western blot **(I)**. Quantitative analyses were shown in the graph (n=3) **(J)**.

**(K-L)** Effects of  $\beta$ -arrestin 1 silencing on the alterations of YAP subcellular localization triggered by INT-777 (2  $\mu$ M) were analyzed using western blot **(K)**. Quantitative analyses were shown in the graph (n=3) **(L)**.

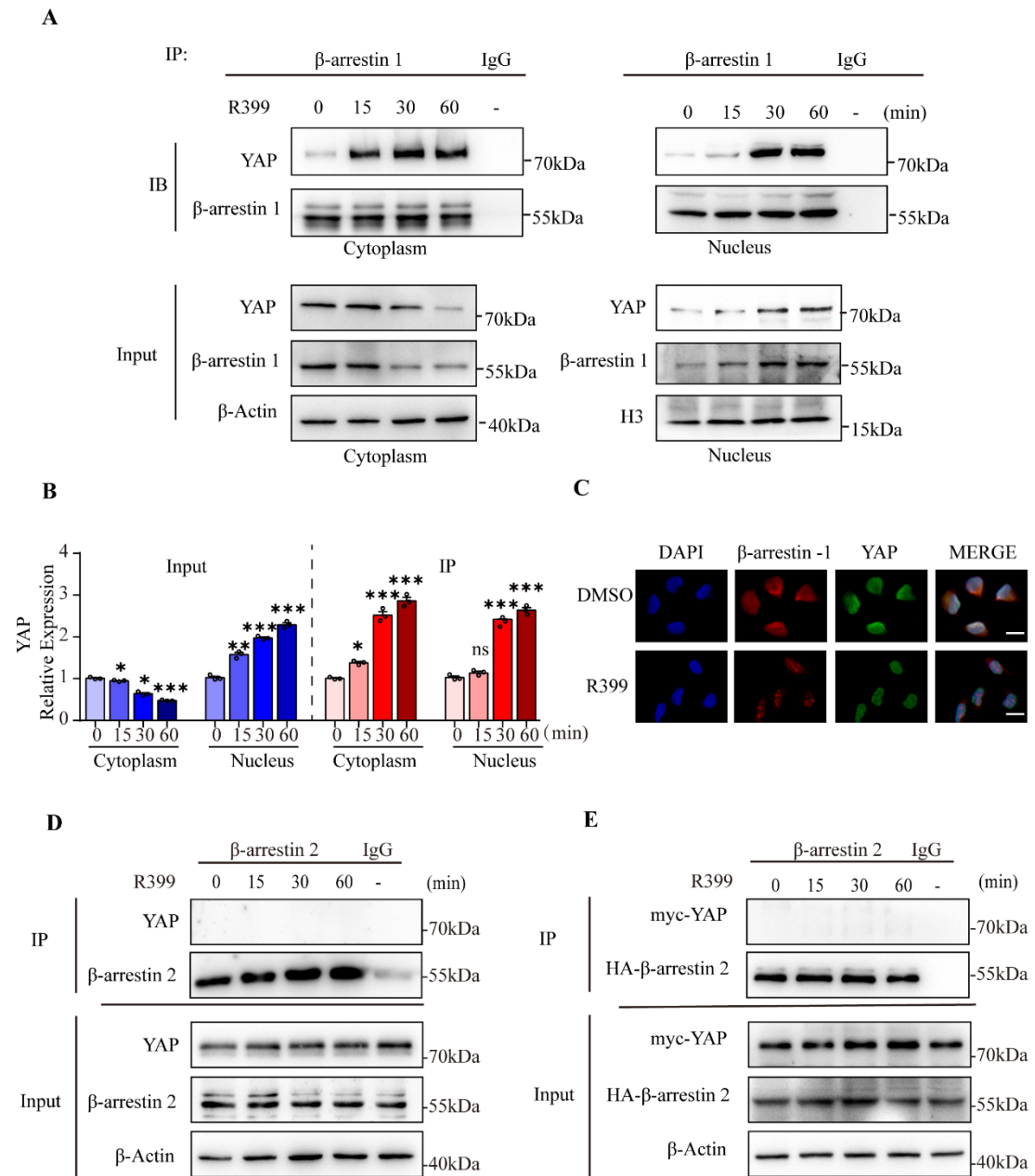
**(M-N)** Effects of Gs inhibitor (NF 449, 10  $\mu$ M), on the alterations of YAP subcellular localization triggered by R399 (700 nM) were analyzed using western blot **(M)**. Quantitative analyses were shown in the graph (n=3) **(N)**.

**(O)** Total extracts of H1299 cells treated with R399 (700 nM) for the indicated time, were immunoprecipitated (IP) for anti- $\beta$ -arrestin 1, or anti-immunoglobulin G (IgG) followed by western blot analysis using anti- $\beta$ -arrestin 1 and anti-YAP.

**(P)** Total extracts of H1299 cells treated with R399 (700 nM) for the indicated time were immunoprecipitated (IP) for anti-YAP or anti-immunoglobulin G (IgG) followed by western blot using anti- $\beta$ -arrestin 1 and anti-YAP.  $\beta$ -Actin was used as loading control.

**(Q)** Schematic of the possible mechanism underlying R399-induced YAP activation.

All data are presented by mean  $\pm$  SEM. ns: not significant, \* $P < 0.05$ , \*\* $P < 0.01$ , \*\*\* $P < 0.001$  based on the Student's t-test. All results are representative of three independent experiments.



**Supplementary Fig. 10 R399 promotes the interaction of  $\beta$ -arrestin 1 and YAP to co-migrate to the nucleus.**

(A-B) Cytoplasmic and nuclear extracts of H1299 cells treated with R399 (700 nM) for the indicated time were immunoprecipitated (IP) for anti- $\beta$ -arrestin 1 or anti-immunoglobulin G (IgG) followed by western blot using anti- $\beta$ -arrestin 1 and anti-YAP.  $\beta$ -Actin

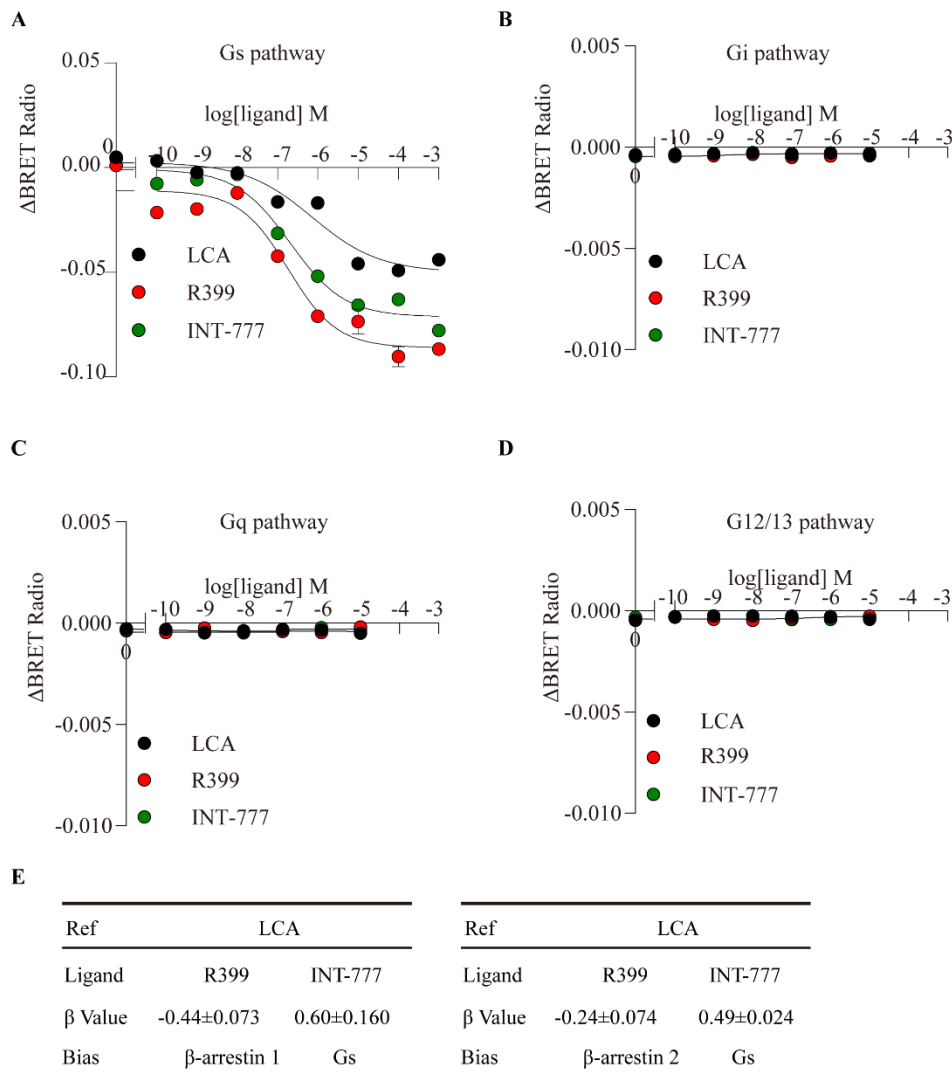
and H3 were used as loading controls **(A)**. Quantitative analyses of YAP detected by western blot were shown in the graph (n=3) **(B)**.

**(C)** Representative immunostaining of  $\beta$ -arrestin 1 and YAP localization in H1299 cells stimulated with DMSO and R399 (700 nM). Nuclei were stained in blue (DAPI).  $\beta$ -arrestin 1 was stained in red. YAP was stained in green. Scale bar: 50  $\mu$ m.

**(D)** Total cellular extracts of H1299 cells treated with R399 (700 nM) for the indicated time were immunoprecipitated (IP) for anti- $\beta$ -arrestin 2, or anti-immunoglobulin G (IgG) followed by western blot analysis using anti- $\beta$ -arrestin 2 or anti-YAP.  $\beta$ -Actin was used as loading control.

**(E)** HEK-293T cells were co-transfected with 4  $\mu$ g of myc-YAP and HA- $\beta$ -arrestin 2. After 48 h, the cells were treated with R399 (700 nM) for the indicated time. Cell lysates were immunoprecipitated with anti-HA-conjugated beads. Co-IPs/lysates and IPs were immunoblotted with antibodies against YAP and HA epitope, respectively.

All data are presented by mean  $\pm$  SEM. ns: not significant, \*P<0.05, \*\*P<0.01, \*\*\*P<0.001 based on the Student's test. All results are representative of three independent experiments.

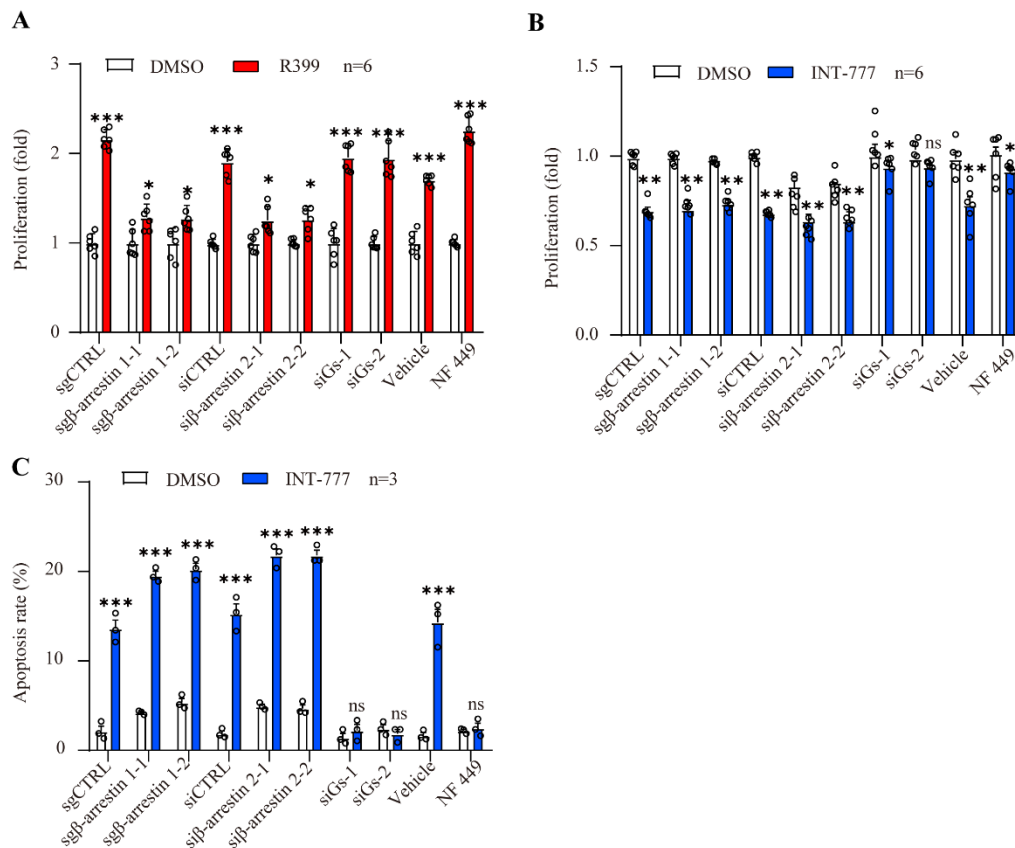


**Supplementary Fig. 11 Gs, Gi, Gq or G12/13 activities in response to LCA, R399 or INT-777 stimulation.**

(A-D) LCA/R399/INT-777–induced Gs (A), Gi (B), Gq (C) and G12/13 (D) activity examined by Gs/Gq/Gi/G12/13-G $\gamma$  dissociation assays, respectively. Data from at least three independent measurements are measured as mean  $\pm$  SEM.

(E) The bias factor ( $\beta$  value) of INT-777 and R399 was calculated using a native bile acid LCA as the reference. The INT-777 is Gs biased ligand with respect to R399.  $\beta >$

0 indicates Gs biased,  $\beta < 0$  indicates  $\beta$ -arrestin 1/2 biased. Data from three independent experiments are presented as mean  $\pm$  SEM.

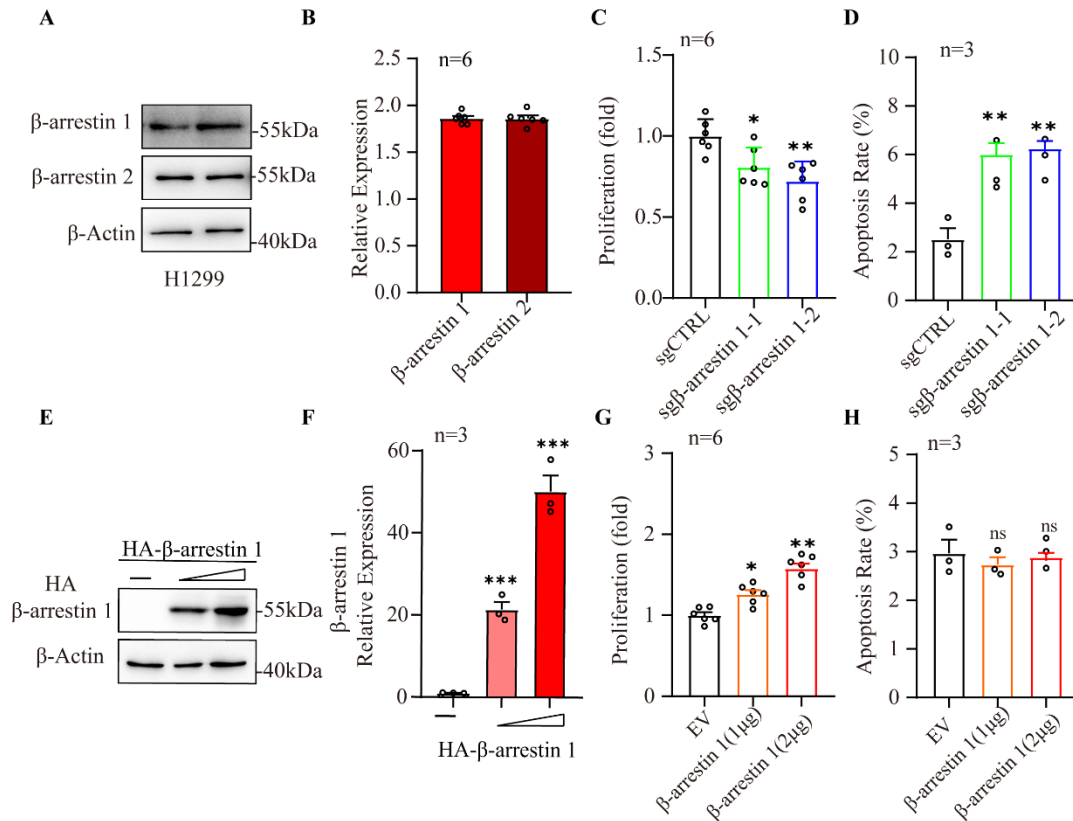


**Supplementary Fig. 12 Gs-bias for INT-777 and β-arrestin-bias for R399 contributed to the distinct biological consequences elicited in NSCLC.**

(A-B) Effects of β-arrestin 1/2 silencing or Gs inhibitor, NF 449 (10 μM), on R399 (A) and INT-777 (B) induced cell growth were evaluated by MTT analysis (n=6).

(C) Following the same settings as in (B), on INT-777-induced cell apoptosis were evaluated by flow cytometry analysis (n=3).

All data are presented by mean ± SEM. ns: not significant, \*P<0.05, \*\*P<0.01, \*\*\*P<0.001 based on the Student's t-test. All results are representative of three independent experiments.



**Supplementary Fig. 13  $\beta$ -arrestin 1 promotes proliferation and inhibits apoptosis in H1299 cells.**

**(A)** The expression of  $\beta$ -arrestin 1 and  $\beta$ -arrestin 2 was examined by western blot in H1299 cells.

**(B)** Quantitative analyses were shown in the graph ( $n=6$ ).

**(C)** MTT analysis was performed to detect the effects of  $\beta$ -arrestin 1 knockdown on cell growth of H1299 cells ( $n=6$ ).

**(D)** Flow cytometry was performed to detect the effects of  $\beta$ -arrestin 1 knockdown on cell apoptosis of H1299 cells ( $n=3$ ).

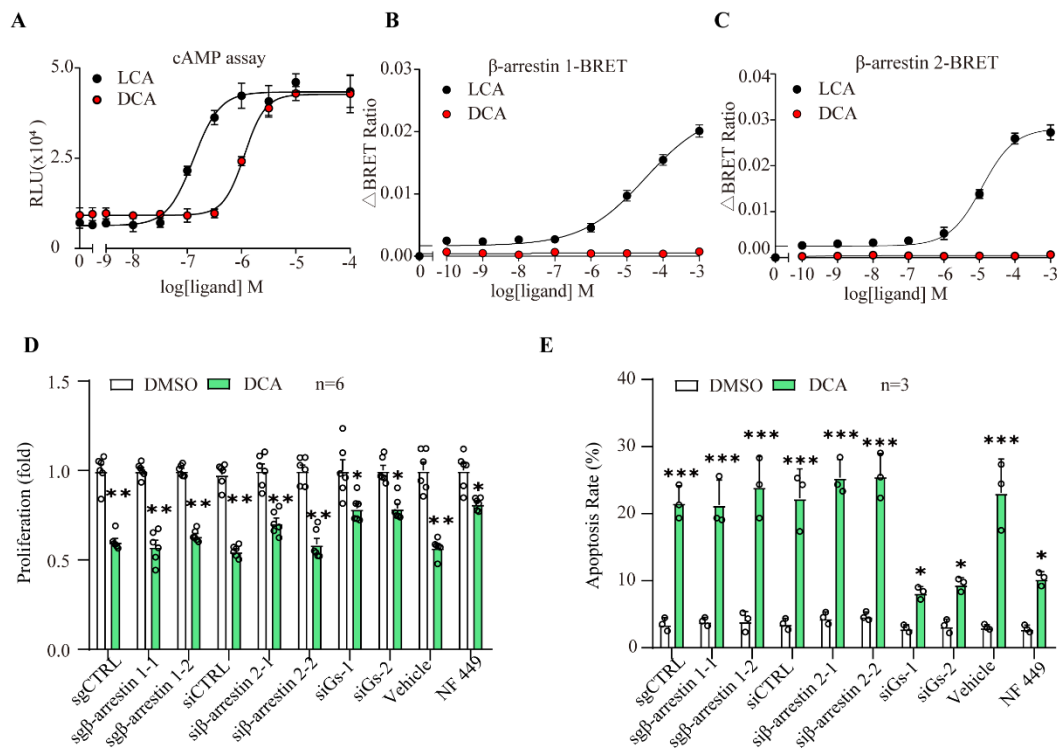
**(E-F)** The protein level of  $\beta$ -arrestin 1 was analyzed by western blot in H1299 cells transfected with  $\beta$ -arrestin 1 expression plasmids (0, 1, 2  $\mu$ g, respectively). Quantitative analyses were shown in the graph ( $n=3$ ).

**(G)** MTT analysis was performed to detect the effects of  $\beta$ -arrestin 1 overexpression on cell growth of H1299 cells ( $n=6$ ).

**(H)** Flow cytometry was performed to detect the effects of  $\beta$ -arrestin 1 overexpression on cell apoptosis of H1299 cells ( $n=3$ ).



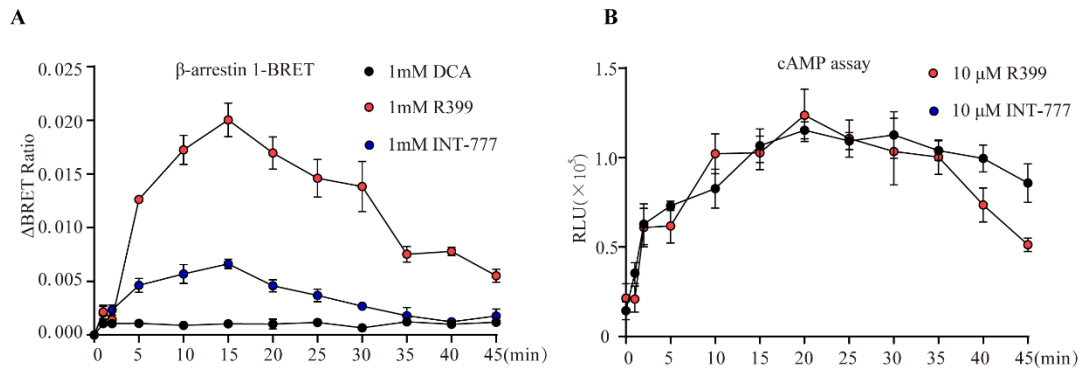
All data are presented by mean  $\pm$  SEM. ns, not significant, \*P<0.05, \*\*P<0.01, \*\*\*P<0.001 based on the Student's t-test. All results are representative of three independent experiments.



**Supplementary Fig. 14 Gs-bias for DCA contributed to the biological consequences in NSCLC.**

(A-C) The biased properties of endogenous agonists DCA and LCA were examined by cAMP accumulation assay (A), β-arrestin 1 (B) and β-arrestin 2 (C) recruitment assay. (D-E) Effects of β-arrestin 1/2 silencing or Gs inhibitor, NF 449 (10 μM), on DCA-induced cell growth and cell apoptosis were evaluated by MTT analysis (n=6) (D) and flow cytometry analysis (n=3) (E).

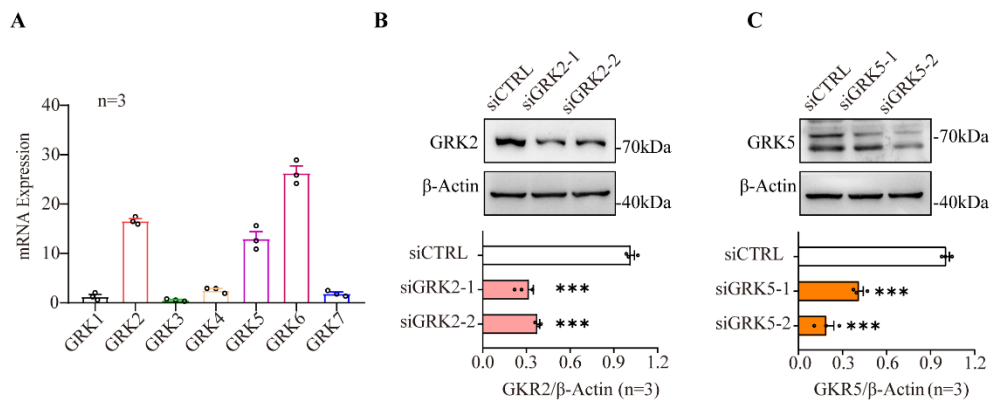
All data are presented by mean ± SEM. ns: not significant, \*P<0.05, \*\*P<0.01, \*\*\*P<0.001 based on the Student's t-test. All results are representative of three independent experiments.



**Supplementary Fig. 15 DCA is a Gs bias ligand of GPBAR.**

**(A)** HEK293 cells were respectively treated with DCA (1 mM), R399 (1 mM) and INT-777 (1mM) for the indicated time. The kinetic responses were monitored by  $\beta$ -arrestin 1 recruitment assay.

**(B)** HEK293 cells were respectively treated with R399 (10  $\mu$ M) and INT-777 (10  $\mu$ M) for the indicated time. The forskolin-induced cAMP accumulation was monitored by Glosensor cAMP assay.

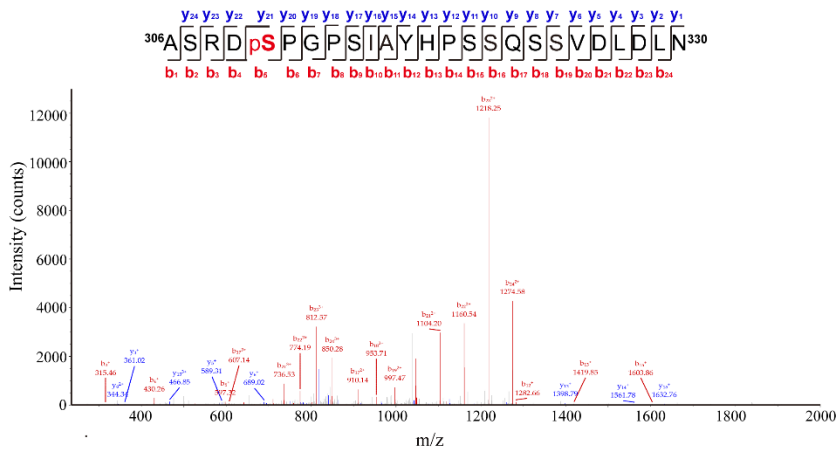
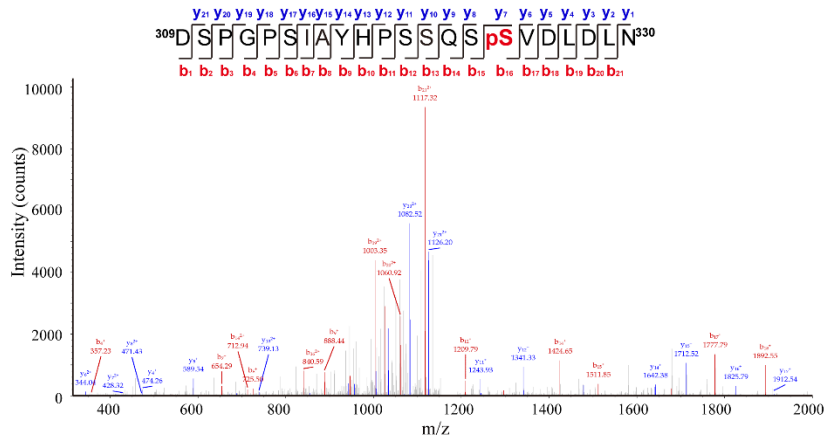
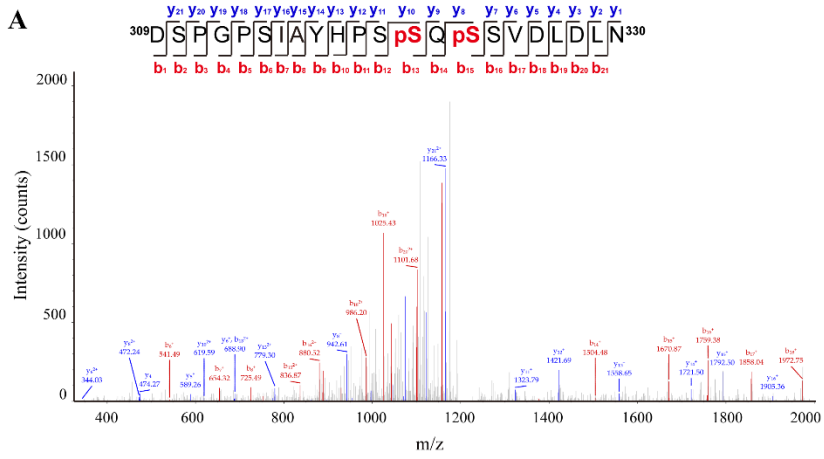
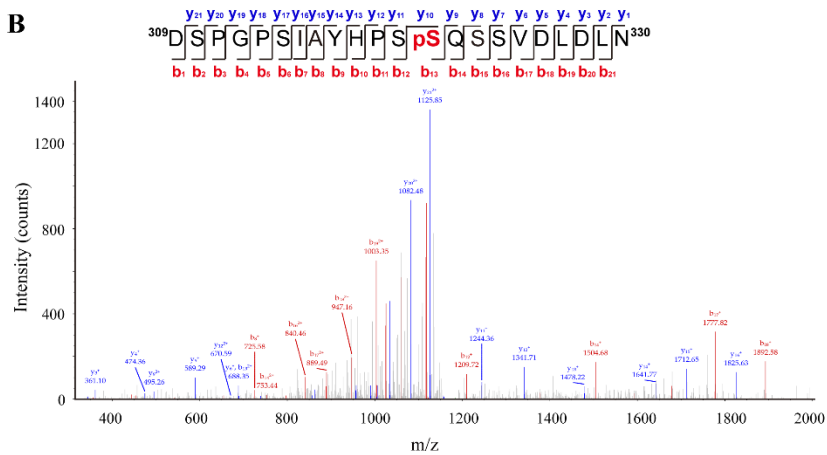


**Supplementary Fig. 16 The protein expression levels of GRK2 and GRK5 transfected with specific siRNAs.**

**(A)** The mRNA levels of GRK1-7 in H1299 cell line were examined by RT-PCR assay (n=3).

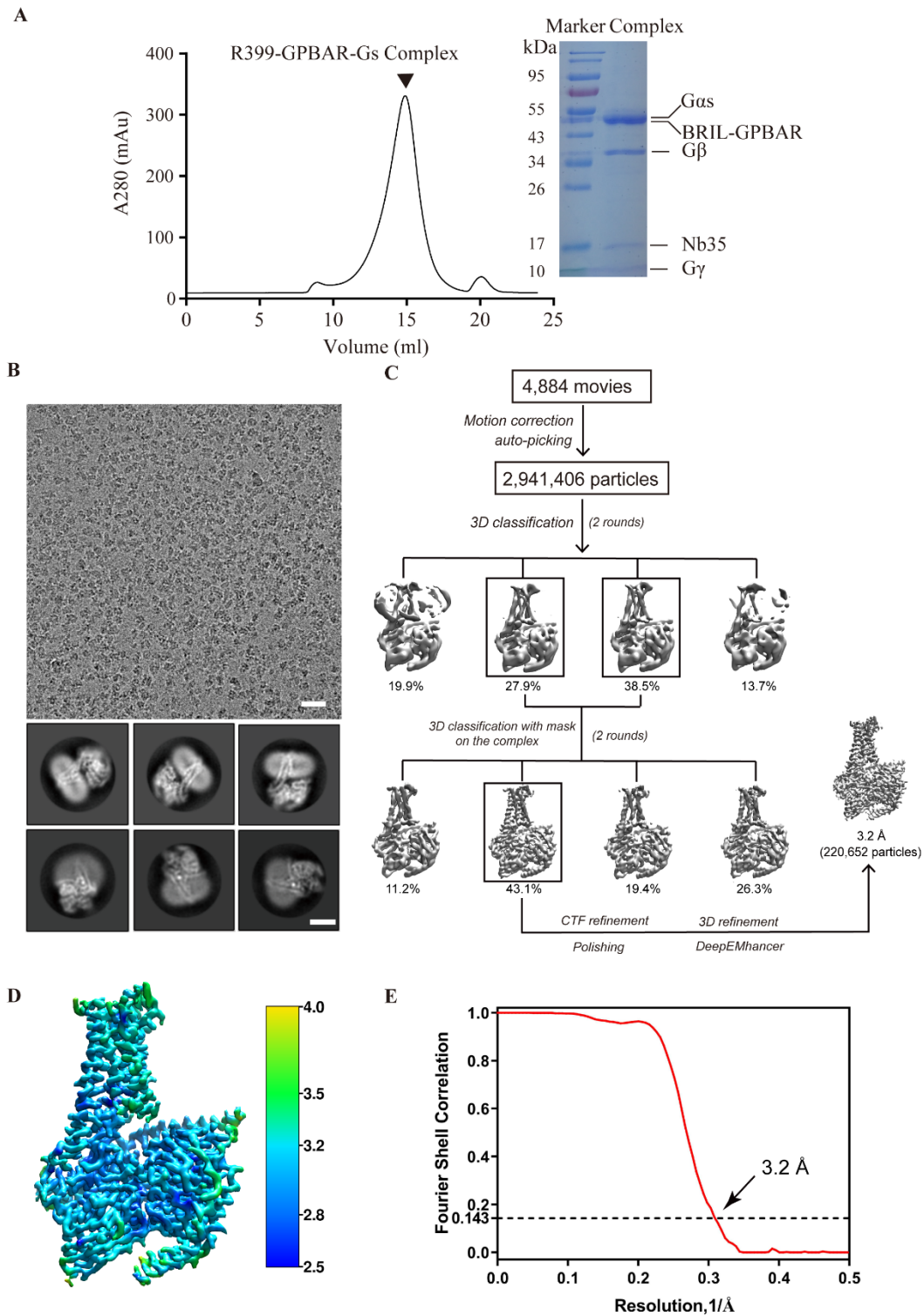
**(B-C)** The protein level of GRK2 and GRK5 were analyzed by western blot transfected with GRK2 **(B)** and GRK5 **(C)** specific siRNAs or siCTRLs. Quantitative analyses were shown in the graph (n=3).

All data are presented by mean  $\pm$  SEM. \*\*\*P<0.001 based on the Student's t-test. All results are representative of three independent experiments.

**A****B**

**Supplementary Fig.17 Phosphorylation sites in GPBAR identified by mass spectrometry (MS).**

**(A-B)** Representative MS/MS spectrum showing phosphorylation sites in GPBAR with siCTRL **(A)** and siGRK2 treatment **(B)**. Both siCTRL and siGRK2 treated cells were stimulated with 700 nM R399 for 5 min before harvesting.



**Supplementary Fig. 18 Cryo-EM images and single particle reconstruction of the R399-GPBAR-Gs complex.**

(A) Representative elution profile of Flag-purified R399-GPBAR-Gs complex on Superose 6 Increase 10/30 column and SDS-PAGE of the size-exclusion chromatography

peak. Thermostable cytochrome b562RIL (BRIL) was introduced into the N-terminal of full-length human GPBAR and co-expressed with Gs protein in *Spodoptera frugiperda* (Sf9) insect cells. By the addition of excess high-affinity agonist R399 and the nanobody Nb35, active complexes were readily formed.

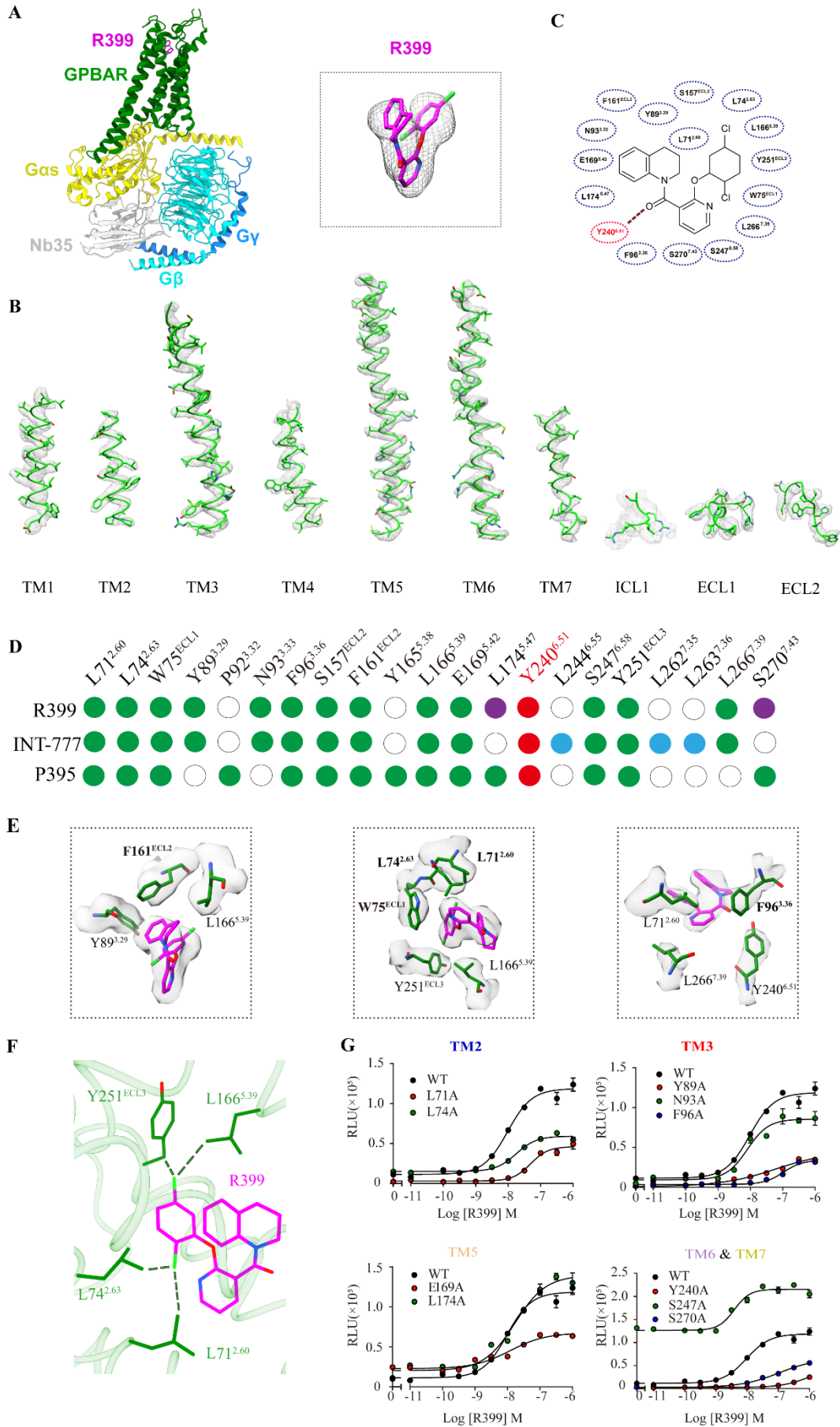
**(B)** Cryo-EM micrograph and reference-free two-dimensional class averages of the R399-GPBAR-Gs complex. Scale bar: 5 nm.

**(C)** Flow chart of cryo-EM data processing of R399-GPBAR-Gs complex. Analysis of the GPBAR-Gs complexes stabilized by R399 enabled us to construct electron density maps with an overall resolution of 3.2 Å.

**(D)** 3D density map colored according to local resolution (Å).

**(E)** An atomic resolution structure of Gold-standard FSC curve (red) of R399 bound GPBAR-Gs complex.





**Supplementary Fig. 19 Selected Cryo-EM density map of R399-GPBAR-Gs complex**

**(A)** Ribbon representation (Left panel) of GPBAR-Gs-R399 complex and cryo-EM density (right panel) of ligand (R399). R399, magentas; GPBAR, green; G $\alpha$ s, yellow; G $\beta$ , cyan; G $\gamma$ , light blue; Nb35, gray.

**(B)** EM density of the transmembrane helices and key intracellular and extracellular loops of R399-GPBAR-Gs complex. GPBAR includes all 7 transmembrane (TM) helices, including intracellular and extracellular loops (ICLs and ECLs, respectively), confidently modeled using high-resolution electron density.

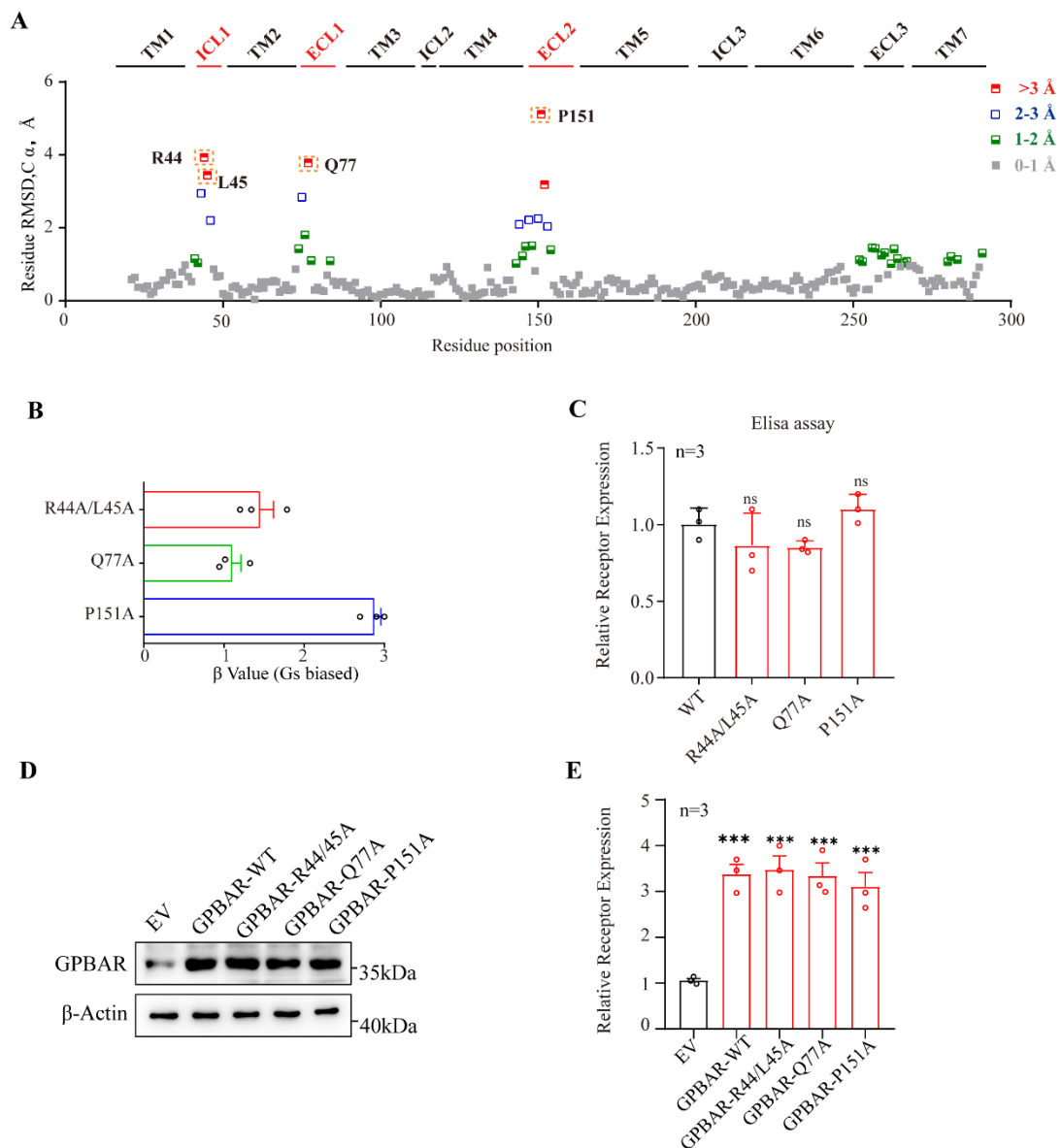
**(C)** Diagram of R399 interaction in the ligand binding pocket of GPBAR. The hydrogen bond is depicted as a red dashed line.

**(D)** Interaction differences in the binding pocket of the GPBAR bound by R399, INT-777 and P395. The residues involved in the hydrogen bond between the ligand and the receptor are marked in red. The residues that interact with the ligand are indicated by green circles, and the residues that do not interact with the ligand are indicated by blank circles. Purple, residues of GPBAR which interact with R399 but not with INT-777; Blue, residues of GPBAR which interact with INT-777 but not with R399. Balles-teros–Weinstein residue numbers are provided for reference.

**(E)** High quality electron density enabled explicit assignment of R399 and several residues surrounding it in different parts of ligand binding pocket.

**(F)** Interaction between two chlorides in the dichlorocyclohexyl group of R399 and GPBAR.

**(G)** Dose response curve of different mutations within the ligand binding pocket of GPBAR on the binding of R399 induced cAMP accumulation in Glosensor assay. Data from at least three independent measurements are measured as mean  $\pm$  SEM.



**Supplementary Fig. 20 Structural basis of the biased agonism by R399.**

**(A)** The distance root mean square deviations (RMSDs) graph of each residual between R399-GPBAR and INT-777-GPBAR structures. The horizontal and vertical axes represent the GPBAR amino acid sequence and RMSDs ( $C\alpha$  deviation) of each residue, respectively. The red, blue, green and grey dots represent  $C\alpha$  deviations that range from  $>3 \text{ \AA}$ ,  $2\sim 3 \text{ \AA}$ ,  $1\sim 2 \text{ \AA}$  or  $<1 \text{ \AA}$ , respectively.

**(B)** Analysis of the biased property of the residuals highlighted in (R44A/L45A, Q77A and P151A)  $\beta$  values calculated from the molecular efficacies of R399.

**(C)** The expression level of wild-type and indicated mutants GPBAR in HEK-293 cells were detected by Elisa experiments.

**(D-E)** The GPBAR protein expression level of wild-type and indicated mutants in A549 cells were detected by western blot, with  $\beta$ -Actin as a loading control **(D)**. Quantitative analyses were shown in the graphs (n=3) **(E)**.

All data are presented by mean  $\pm$  SEM. ns: not significant, \*\*\*P<0.001 based on the Student's t-test. All results are representative of three independent experiments.

## Supplementary Tables

**Table S1 Genetic diversity of non-small cell lung cancer cells**

Cell lines	EGFR status	KRAS status	TP53 status	Histology
H1299	Wild type	Wild type	NULL	Adenocarcinoma
H1975	L858R+T790M	Wild type	R273H	Adenocarcinoma
95D	Wild type	Wild type	Wild type	Adenocarcinoma
Anip973	Wild type	Wild type	Wild type	Adenocarcinoma
HCC827	Del(E746-A750)	Wild type	Wild type	Adenocarcinoma
H520	Wild type	NULL	W146	Squamous cell carcinoma
A549	Wild type	G12S	Wild type	Adenocarcinoma
PC9	Del(E746-A750)	Wild type	Wild type	Adenocarcinoma

**Table S2 Interaction of R399 binding pockets**

Interaction	Amino acid	Distance (Å)
H-bond ( $\leq 3.2$ Å)	Y240	3.1
Hydrophobic ( $\leq 4.0$ Å)	L71	3.2
	L74	3.0
	W75	3.8
	F96	3.7
	S157	4.0
	F161	3.7
	L166	3.2
	E169	3.8
	L174	3.6
	Y251	3.4
	L266	3.7
Vanderwals force ( $\leq 4.0$ Å)	N93	3.9
	S247	3.9
	S270	2.8
$\pi$ - $\pi$ stacking (Edge- $\pi$ , $\leq 8.0$ Å)	Y89	5.3

**Table S3 Sequences of shRNA/siRNA/sgRNA used in this study**

Name	Sequence (5'--3')
shCTRL	GTTCTCCGAACGTGTCACGT
GPBAR-shRNA-1	CGTCTACTTGGCTCCCAACTT
GPBAR-shRNA-2	CCTCATCATCACCGCGAACCT
Negative control (siCTRL)	UUCUCCGAACGUGUCACGUTT
	ACGUGACACGUUCGGAGAATT
GPBAR-siRNA-1	GUCUGGCAUUGCCCACAUUTT
	AAUGUGGGCAAUGCCAGACTT
GPBAR- siRNA-2	UCUACUUGGCUCCCAACUUTT
	AAGUUGGGAGCCAAGUAGATT
$\beta$ -arrestin 2-siRNA-1	CCACCAAGACCGUCAAGAATT
	UUCUUGACGGUCUUGGUGGTT
$\beta$ -arrestin 2-siRNA-2	ACACGCCACUUCCUCAUGUTT
	ACAUGAGGAAGUGGCGUGUTT
Gs-siRNA-1	AGCAGATGAGGATCCTGCATGTAA
	UUAACAUGCAGGAUCCUCAUCUGCU
Gs-siRNA-2	CCUGAAAGAGGGCGAUUGAAACCAU
	AAUGGUUCAAUCGCCUCUUUCAGG
YAP-siRNA-1	CCAAUAGCUCAGAUCCUUUTT
	AAAGGAUCUGAGCUAUUGGUC
YAP-siRNA-2	GCAUC UUCGACAGUCUUCUTT
	AGAAGACUGU CGAAGAUGCTT
GRK2-siRNA-1	GCCCUUGGUGGAAUUCUAUTT
	AUAGAAUCCACCAAGGGCTT
GRK2-siRNA-2	CCAUACAUCGAAGAGAUUUTT
	AAAUCUCUUCGAUGUAUGGTT
GRK5-siRNA-1	GGACCAUAGACAGAGAUUATT
	UAAUCUCUGUCUAUGGUCCTT
GRK5-siRNA-2	GCCUCAUCUAUGAGAUGAUTT
	AUCAUCUCAUAGAUGAGGCTT
sg $\beta$ -arrestin 1-1	CACCGACGTACAGTCGTTCCCACCG
	AAACCGGTGGGAACGACTGTACGTC
sg $\beta$ -arrestin 1-2	CACCGCAACGTACAGTCGTTCCCAC
	AAACGTGGGAACGACTGGTACGTTGC

**Table S4 Primers used for qRT-PCR**

<b>Gene</b>	<b>Primer</b>	<b>Sequence (5' --3' )</b>
β-actin	Forward	AGTTGCGTTACACCCTTTCTTG
	Reverse	CACCTTCACCGTTCAGTTTT
CDX2	Forward	CCAATGACAACGCCTCCTG
	Reverse	TGGTGCAGCCAGAAAGCTC
CTGF	Forward	AAAAGTGCATCCGTACTIONCCA
	Reverse	CCGTCGGTACATACTCCACAG
CYR61	Forward	AGCCTCGCATCCTATAACAACC
	Reverse	TTCTTTCACAAGGCGGCACTC
CDC2	Forward	GACCACTCCTAGCAAACCTGG
	Reverse	GGGCGTCTGGCTGTTTTCA
NKRD1	Forward	CACTTCTAGCCCACCCTGTGA
	Reverse	CCACAGGTTCCGTAATGATTT
TAGLN	Forward	CCCGAGAACCCACCCTCCA
	Reverse	AAAGCCATCAGGGTCCTCTGC
EDN1	Forward	TGTGTCTACTTCTGCCACCT
	Reverse	CCCTGAGTTCTTTTCCTGCTT
PPP1R3B	Forward	GGACACGTTCTCCTTCGAC
	Reverse	AGATTTTAACTCAGCCCGGAT
EGR3	Forward	GCAGCGACCACCTCACCAC
	Reverse	CCGCCTTCTTCTCCTTTTGCT
EGR4	Forward	CGACGAGCTCAATCGCCACCT
	Reverse	GCCGCACACGTCGCAAGCA



**Table S5 The types, dilutions and sources of antibodies used for western blot, immunohistochemistry (IHC) and immunofluorescence (IF) analysis**

Antibody	Working dilution	Working dilution	Species	Source and Cat.Number
	western blot	IHC/IF		
GPBAR	1:1000	-	Rabbit polyclonal	Abcam (Cat. No. Ab72608)
PARP1	1:2000	-	Rabbit polyclonal	Proteintech (Cat.No.13371-1-AP)
Cleaved-Caspase3	1:1000	1:100	Rabbit monoclonal	Cell Signaling Technology (Cat.No.9661)
Ki-67	-	1:100	Rabbit monoclonal	Abcam (Cat. No. ab15580)
CK7	-	1:100	Rabbit monoclonal	Abcam (Cat. No. ab199718)
TTF-1	-	1:100	Mouse monoclonal	Cell Signaling Technology (Cat.No.23192)
Napsin A	-	1:100	Rabbit monoclonal	Cell Signaling Technology (Cat.No.62434)
$\beta$ -arrestin 1	1:1000	-	Rabbit monoclonal	Cell Signaling Technology (Cat.No.30036)
$\beta$ -arrestin 2	1:1000	-	Rabbit monoclonal	Cell Signaling Technology (Cat.No.3857)
YAP	1:1000	-	Rabbit monoclonal	Cell Signaling Technology (Cat.No.14074)
Phospho-YAP (Ser127)	1:1000	-	Rabbit monoclonal	Cell Signaling Technology (Cat.No.13008)
Histone H3	1:1000	-	Rabbit monoclonal	Cell Signaling Technology (Cat.No.4499)
GRK2	1:1000	-	Mouse polyclonal	Santa Cruz Biotechnology (Cat.No.SC-13143)
GRK5	1:1000	-	Rabbit monoclonal	Proteintech (Cat.No.17032-1-AP)
$\beta$ -Actin	1:3000	-	Mouse polyclonal	Cell Signaling Technology (Cat.No. ab64659)
FLAG	1:1000	-	Mouse monoclonal	Sigma Aldrich (Cat.No. F1804)

Secondary anti-body	1:1000	-	Mouse monoclonal	Abcam (Cat. No. ab205719)
Secondary anti-body	1:1000	-	Rabbit monoclonal	Sigma-Aldrich (Cat.No. A6154)
Donkey anti-Mouse IgG (H+L) Highly Cross-Adsorbed Secondary Antibody, Alexa Fluor 568	-	1:100		Thermo Fisher Scientific (Cat.No. A10037)
Donkey anti-Rabbit IgG (H+L) Highly Cross-Adsorbed Secondary Antibody, Alexa Fluor Plus 488	-	1:100		Thermo Fisher Scientific (Cat.No. A32790)

**Table S6 The types and sources of agonists of GPBAR and YAP as well as the inhibitors of YAP, FXR and Gs.**

<b>Agonists/inhibitors</b>	<b>Source and Cat.Number</b>
Cholic acid (CA)	SIGMA C1129
Deoxycholic acid (DCA)	SIGMA D2510
Ursodeoxycholic acid (UDCA)	SIGMA U5127
Chenodeoxycholic acid (CDCA)	SIGMA C9377
Taurocholic acid sodium salt hydrate (TCA)	SIGMA T4009
Sodium taurodeoxycholate hydrate (TDCA)	SIGMA T0875
Glycocholic acid hydrate (GCA)	SIGMA G2878
Lithocholic acid (LCA)	SIGMA L6250
INT-777	MCE HY-15677/CS-3199
PY-60	MCE HY-141644
MYF-01-37	MCE HY-139603
T- $\beta$ MCA sodium	MCE HY-135105
NF 449	MCE HY-112461A

**Table S7 Cryo-EM data collection, model refinement and validation statistics**

	399-GPBAR-Gs
<b>Data collection and processing</b>	
Magnification	4,9310
Voltage (kV)	300
Electron exposure (e <sup>-</sup> /Å <sup>2</sup> )	64
Defocus range (μm)	-0.5 ~ -2.5
Pixel size (Å)	1.014
Symmetry imposed	C1
Initial particle projections (no.)	2,941,406
Final particle projections (no.)	220,652
Map resolution (Å)	3.2
FSC threshold	0.143
Map resolution range (Å)	2.5-4.0
<b>Refinement</b>	
Initial model used (PDB code)	7CFM
Model resolution (Å)	3.5
FSC threshold	0.5
Model resolution range (Å)	2.5-5.0
Map sharpening method	DeepEMhancer
Model composition	
Non-hydrogen atoms	8010
Protein residues	1027
Ligand	1
<i>B</i> factors (Å <sup>2</sup> )	
Protein	66.79
Ligand	69.79
R.m.s. deviations	
Bond lengths (Å)	0.004
Bond angles (°)	0.729
Validation	
MolProbity score	1.48
Clashscore	5.53
Rotamer outliers (%)	0.00
Ramachandran plot	
Favored (%)	96.94
Allowed (%)	3.06
Disallowed (%)	0

## **Supplemental Methods and Materials**

### **Cell culture and transfection**

The human NSCLC cell lines H1299, H1975, A549 and PC9 were purchased from the Cell Bank of the Chinese Academy of Science (Shanghai, China) and cultured in RPMI-1640 medium containing 10% fetal bovine serum (FBS), together with 100 mg/mL streptomycin and 100 U/mL penicillin. The cells were maintained in humidified incubator containing 5% CO<sub>2</sub> /95% air atmosphere at 37°C and were resuscitated every 3 months and tested negative for mycoplasma contamination. For all transfection procedures, standard protocols were followed in accordance with manufacturer's instructions using Lipofectamine 2000 (Invitrogen).

### **Generation of GPBAR stable knockdown cell lines**

Lentivirus transduction system was utilized to generate GPBAR stable silencing cells as previously described (1). shRNA sequence information was provided in **Table S3**. The expression of GPBAR was further confirmed by western blot.

### **Expression plasmids**

Human GPBAR gene (GPBAR1) was cloned into both mammalian and insect cell expression vectors. For GRK2, GRK5 and GRK6 were cloned into pcDNA3.1 (Invitrogen). To facilitate expression and purification, an N-terminal BRIL epitope was inserted after Flag tag (DYKDDDDK). A dominant-negative G $\alpha$ s (S54N, G226A, E268A, N271K, K274D, R280K, T284D, I285T) (2-5) was generated by Quikchange mutagenesis kit (Stratagene) and was cloned into insect cell expression. The human G $\beta$ 1 containing the N-terminal 6 $\times$ His tag and 3C protease site and the human G $\gamma$ 2 were cloned into pFastbac dual vector. Using the Quikchange mutagenesis kit (Stratagene) generates all the GPBAR mutations used for functional studies. pCMV-Myc-YAP plasmid was a generous gift from Dr. Tao Zhang. 8 $\times$ GTIIC-luciferase plasmid was purchased from Addgene, a non-profit plasmid repository (<http://www.addgene.org/>). sgRNAs specific for  $\beta$ -arrestin 1 and corresponding negative control RNAs were constructed to PX458 and plenti-CRISPR-V2 vectors. shRNAs specific for GPBAR were cloned into pLKO.1-TRC vector (GenePharma). siRNAs specifically targeting GPBAR,  $\beta$ -arrestin

1/2 and Gs as well as the negative controls were purchased from GenePharma (Shanghai, China). The sequences of aforementioned oligonucleotides were listed in **Table S3**.

### **RNA sequencing and data analysis**

Total RNA was extracted using TRIzol reagent (Invitrogen), quantified and quality controlled using a 2100 Bioanalyzer (Agilent). RNA samples with RNA Integrity Number (RIN) above 7 were depleted for ribosomal RNA and converted into cDNA library using a TruSeq Stranded Total Library Preparation kit (Illumina). The cDNA library was then sequenced on the Illumina NovaSeq 6000 to generate 150 bp pair-end reads, which were mapped to the human genome using hisat2 (v2.0.0) after quality control filtering. The differential gene expression among different groups was identified using Limma packages (v3.3.5). The list of pre-ranked genes was subjected for KEGG gene set enrichment pathway analysis. Significantly enriched terms were identified using a false discovery rate q value of less than 0.05.

### **Quantitative real time PCR (qRT-PCR)**

Total RNAs were isolated using the Trizol reagent (Invitrogen). Reverse transcription was carried out using the SuperScript III Reverse Transcriptase kit (Invitrogen). Real time PCR was performed using qPCR SYBR Green master mix (Takara Bio) on a CFX Connect Real-time PCR Detection System (Bio-Rad).  $\beta$ -Actin was used as an internal control for RNA expression normalization using the  $2^{-\Delta\Delta C_t}$  method. Sequence information for primers used for qRT-PCR is provided in **Table S4**.

### **Antibodies and reagents**

The antibodies used in our experiments were listed in **Table S5**. The agonists of GPBAR used in our experiments were listed in **Table S6**. Verteporfin (YAP inhibitor, VP) was a kind gift from Dr. Wenwen Liu.

### **Luciferase reporter assay**

Luminescence was measured using Dual Luciferase Reporter Assay System (Promega Corporation) according to manufacturer's instructions. Cells were washed with PBS and lysed in passive lysis buffer from the kit. Luminescence was measured using the Multimode plate reader (PerkinElmer EnVision). Luminescence was normal-

ized to Renilla luciferase activity and was displayed as the average of the three replicates.

### **Cell proliferation assay**

Cells were seeded in 96-well plates at 2,000 cells per well. Cell proliferation was analyzed by 3-(4, 5-dimethylthiazol-2-yl)-2, 5-diphenyltetrazolium bromide (MTT) (Sigma Aldrich) at different times after drug treatment. The MTT assay was performed by adding 10  $\mu$ L MTT (5mg/mL) into each well for 4 h after which particles were dissolved using DMSO. Absorbance was measured at 490 nm on a microplate reader.

### **Flow cytometry for cell apoptosis**

Cell apoptosis was detected using Annexin V-FITC/PI apoptosis detection kit (Vazyme).  $2 \times 10^5$  cells were seeded in 6 well plates and treated with DCA, INT-777, R399 or DMSO for 24 h. Then, cells were collected and resuspended in 100  $\mu$ L Binding Buffer, followed by staining with 5  $\mu$ L Annexin V-FITC and 5  $\mu$ L propidium iodide (PI) for 10 min at room temperature in the dark and fluorescence-activated cell sorter (FACS) was used for quantification.

### **Terminal dUTP nick-end labeling (TUNEL) assay**

To detect DNA fragmentation, TUNEL staining was performed using TUNEL BrightGreen Apoptosis Detection Kit (Vazyme) and TUNEL BrightRed Apoptosis Detection Kit (KeyGen) according to manufacturer's instructions. In short, well-fixed and permeabilized cells on the slide were labeled in 50  $\mu$ L of TdT reaction buffer at 37°C for 1 h in a moist, dark chamber. Counterstaining was performed with Antifade Mounting Medium containing 2  $\mu$ g/mL DAPI (Beyotime). The samples were analyzed under a fluorescence microscope (Axio Scope A1) with standard light filters and ZEN connected software. Data were presented as the ratio of TUNEL-positive cells (%).

### **Immunoblotting and Immunoprecipitation (IP)**

For western blot analysis, total cell extracts were prepared in RIPA buffer (Thermo Fisher Scientific) supplemented with protease inhibitors (Roche) and phosphatase inhibitors (Solarbio). Nuclear and cytoplasmic extracts were prepared using a nuclear and cytoplasmic protein extraction kit (Beyotime Biotechnology) according to the manu-

facturer's instructions. Protein samples were separated by 8-12% SDS-PAGE and electrically transferred to polyvinylidene fluoride (PVDF) membrane (Millipore). The membranes were probed with indicated primary and secondary antibodies detailed in **Table S5**. For co-immunoprecipitation, total cell extracts were prepared in IP Lysis Buffer supplemented with protease inhibitor (Roche). Pre-cleared whole cell lysates or cytoplasmic and nuclear cell fractions were incubated with the indicated target-specific antibody overnight at 4 °C in a rotating wheel, followed by incubation with PureProteome™ Protein A/G Mix Magnetic Beads (Millipore) for 2h at 4°C and 30 min at room temperature with rotation. Immunoprecipitates were analyzed by SDS-PAGE and western blot.

### **Protein biotinylation and receptor expression examination**

To detect the membrane expression of GPBAR, cell surface biotinylation assay were performed using EZ-Link Sulfo-NHS-SS-Biotin (Thermo Scientific 21331) following the manufacturer's instructions. GPBAR silencing cells (siGPBAR) and their control cells were washed with cold PBS for three times. Then, cells were suspended at a concentration of  $3 \times 10^7$  cells/mL in PBS containing 10 mM solution of EZ-link Sulfo-NHS-SS-Biotin (ThermoFisher) for 30 min at room temperature with end to end rotation. To quench any non-reacted biotinylation reagent, 30 mM Tris was used for the initial wash. Cells were washed with cold PBS for three times at 4 °C. Cell extracts were lysed by 0.5% (w/v) LMNG (Anatrace) and 0.1% (w/v) CHS (Anatrace) supplemented with Protease Inhibitor Cocktail (Roche) for 2 h at 4 °C with end to end rotation. After 20,000×g centrifugation at 4 °C, non-solubilized material was removed. Then, supernatant was incubated with prewashed High Capacity NeutrAvidin® Agarose Resins (ThermoFisher) for 1 h at 4 °C with end to end rotation. Beads were washed three times with cold PBS and SDS loading buffer (Invitrogen) was added to beads. The surface expression of GPBAR was analyzed by western blot using anti-GPBAR antibody (Abcam).



### **Immunofluorescence assay**

Immunofluorescent staining of cells was performed as previously described (6). All images were taken with the same exposure time and processed with same standard.

### **Patient information and tissue specimens**

The 28 pairs of NSCLC and adjacent non-tumor samples were used in this study which was diagnosed by pathological examination at the Second Hospital of Shandong University in 2021. All individuals had been informed the purpose of our research and signed consent on the medical research use of their personal information and specimens according the authorization of the Institutional Research Ethics Committee. The clinical stages of NSCLC were described using the tumor-node-metastases (TNM) cancer staging system announced by the International Union for Cancer Control (UICC).

### **Immunohistochemistry (IHC)**

For IHC staining, xenograft tumor samples and lung tissues were fixed with formalin and embedded in paraffin. The sliced sections were processed and stained as described previously (7). Images were obtained using an upright microscope (Olympus Microsystems) and the scoring methods were described in our previous study (8). The scoring results were analyzed by two experienced pathologists.

### **Nude mice xenograft model**

Nude mice (5 weeks old) were purchased from Beijing Laboratory Animal Co. Ltd. , and maintained in microisolator cages. All animals were used in accordance with institutional guidelines and the current experiments were approved by the Use Committee for Animal Care of Shandong University. To establish Xenograft model, GPBAR stable silencing cells (shGPBAR) and their control cells (shCTRL,  $5 \times 10^5$ ) were, respectively, injected subcutaneously into the axilla of each nude mouse. Ten days later, the volume of the tumors reached about 5 mm in diameter. The mice inoculated with shGPBAR or shCTRL cells were divided randomly into the following 3 groups that received either vehicle control (DMSO), 30 mg/kg INT-777, or 9 mg/kg R399 (n=5 per group) intraperitoneally every three days for thirty days. The body weight and two perpendicular tumor diameters were measured every 3 days. Tumor growth was plotted as tumor volume versus time since inoculation. At termination, tumors were excised,

weighed, and photographed.

### **Mass spectrometry**

The GRK2-phosphorylated GPBAR proteins were electrophoretized, and the protein bands were cut into small plugs. The gel was dehydrated in acetonitrile for 10 min, and then dried in Speedvac (Labconco) for about 15 min. Disulfide bonds were reduced with dithiothreitol (DTT), alkylated with 40 mM IAA and 25 mM  $\text{NH}_4\text{HCO}_3$  in the dark for 45 min. Then, the samples were digested by trypsin at 37 °C for 14 h, 1% (v/v) formic acid stopped the reaction. After digestion, samples were purified, desalted, and dissolved in 30  $\mu\text{L}$  50% (v/v) acetonitrile /0.1% (v/v) trifluoroacetic acid buffer, and analyzed by MS/MS. The data were performed using Bioworks 3.2 software. For the determination of the phosphorylated sites in GPBAR, samples were treated with PNGase F and immediately followed by electrophoresis and tandem mass spectrometry analysis.

### **Protein expression**

Sf9 cells were cultured in ESF 921 serum-free media (Expression System) to a density of  $2.5 \times 10^6$  cells per ml and then were co-infected with GPBAR, Gas and G $\beta$ 1 $\gamma$ 2 (Bac-to-Bac Baculovirus system, Invitrogen) at a ratio of 1:2:2 per liter at 27 °C for 48 h. Then, cells were collected through centrifugation and the obtained cell pellets were stored at -80 °C.

### **Complex purification**

Buffer solution was first prepared with 20 mM HEPES pH 7.5, 100 mM NaCl, 3 mM  $\text{MgCl}_2$  and complete Protease Inhibitor Cocktail Tablets (Roche). This buffer is then used to resuspend cell pellets. After adding 10  $\mu\text{M}$  R399, Nb35-His (10  $\mu\text{g}/\text{mL}$ ) and apyrase (25 mU/mL, NEB), the complex began to form. After incubation at room temperature for one hour, the suspension was solubilized by a buffer containing 0.5% (w/v) lauryl maltose neopentyl glycol (LMNG, Anatrace) and 0.05% (w/v) cholesteryl for 2 h. The supernatant was extracted by centrifugation at 65000g for 30 min, and the solubilized complex was immobilized using M1 anti-Flag affinity resin containing 5mM  $\text{CaCl}_2$ . The resin was filled into a glass column and washed with 30 column volumes of wash buffer containing 20 mM HEPES pH 7.5, 100 mM NaCl, 3 mM  $\text{MgCl}_2$ ,

5 mM CaCl<sub>2</sub>, 10 μM R399, 0.01% (w/v) LMNG and 0.001% (w/v) CHS before bound material was eluted with 10 mM EGTA and 0.2 mg/mL FLAG peptide (Shanghai Qiangyao Biotechnology Co., Ltd.). The complex was concentrated through an Amicon Ultra Centrifugal Filter (MWCO, 100 kDa) and subjected to size-exclusion chromatography on a Superdex 200 Increase 10/300 column (GE Healthcare) that was pre-equilibrated with a buffer containing 20 mM HEPES pH 7.5, 100 mM NaCl, 3 mM MgCl<sub>2</sub>, 10 μM R399, 0.00075% (w/v) MNG, 0.00025% glyco-diosgenin (GDN, Anatrace) and 0.0001% (w/v) CHS to extract complex from contaminants. The elution component consists of a receptor and G protein complex. In insect cell culture, the final yield of purified complex was about 0.45 mg/L.

### **G $\alpha$ -G $\gamma$ dissociation assay**

The G $\alpha$  dissociation from G $\beta\gamma$  assay was performed as previously described (9, 10). Briefly, the plasmids Flag-GPBAR, Nanoluc-G $\alpha$ , His-G $\beta$ 1 and GFP10-G $\gamma$ 2 were transiently co-transfected into HEK293 cells using Lipofectamine 2000 (Thermo Fisher Scientific). After 36 h transfection, the cells were digested, centrifuged, washed twice with BRET buffer (25 mM Hepes, 1 mM CaCl<sub>2</sub>, 140 mM NaCl, 2.7 mM KCl, 0.9 mM MgCl<sub>2</sub>, 0.37 mM NaH<sub>2</sub>PO<sub>4</sub>, 5.5 mM D-glucose, 12 mM NaHCO<sub>3</sub>, pH=7) and resuspended in 500 μLBRET buffer. After dividing the cells into 96-well white plates at 1×10<sup>5</sup> cells per well, Luciferase substrate coelenterazine 400a (5 μM) and ligand were added. Data were read in the Mithras LB940 microplate reader (Berthold Technologies), which was equipped with 400 nm excitation and 515 nm emission filters. The BRET signal was represented by calculating the ratio of the light emitted by GFP2 and the light emitted by Nanoluc.

### **Cryo-EM data acquisition**

For the preparation of Cryo-EM grids, the purified R399-GPBAR-Gs complex at 5.0 mg/mL was applied onto a glow-discharged holey carbon grid (Quantifoil R1.2/1.3, 200 mesh) and subsequently vitrified using a Vitrobot Mark IV (Thermo Fischer Scientific). Cryo-EM data collection was performed on a Titan Krios at 300 kV accelerating voltage in the Center of Cryo-Electron Microscopy, Zhejiang University (Hangzhou, China). Micrographs were recorded using a Gatan K2 Summit detector in counting mode with a pixel size of 1.014 Å using the SerialEM software. Image stacks were

obtained at a dose rate of  $8.0 \text{ e}/\text{\AA}^2/\text{s}$  with a defocus ranging from  $-1.0$  to  $-2.5 \text{ }\mu\text{m}$ . The total exposure time was  $8 \text{ s}$  and  $40$  frames were recorded per micrograph. A total of  $4884$  movies were collected for the complex.

### **Elisa assay**

After transfected wild type GPBAR or its mutants for  $24 \text{ h}$ , cells were seeded at a density of  $40000$  cells/well into  $96$ -well plates and were reared at  $37 \text{ }^\circ\text{C}$  in  $5\% \text{ CO}_2$  atmosphere for another  $24 \text{ h}$ . Cells blocked by  $5\%$  (w/v) BSA for at least  $1 \text{ h}$  at room temperature, before cells adhere to the plate by polyformaldehyde for  $10 \text{ min}$ . The washed Elisa plates were reared with the monoclonal anti-FLAG and then horseradish peroxidase (HRP) -conjugated anti-mouse antibody for  $1 \text{ h}$ , respectively. After washing the plates iteratively and adding with TMB substrate, the plates were quenched by  $0.25 \text{ M HCl}$ . The absorbance at  $450 \text{ nm}$  was determined and the background binding of the phage was monitored by the absorbance from the control wells.

### **cAMP accumulation assay**

The GloSensor cAMP assay was as described above (11, 12). FLAG-tagged wild type human GPBAR/its mutants and the GloSensor plasmid were transfected into HEK293 cells, and then HEK293 cells were seeded at a density of  $40000$  cells /well into  $96$ -well culture plates and reared for  $48 \text{ h}$  at  $37 \text{ }^\circ\text{C}$  in  $5\% \text{ CO}_2$ . Cells were conducted by starvation of serum-free media which contained  $5\%$  v/v dilution of the GloSensor™ cAMP reagent stock solution (Progema) for  $2 \text{ h}$ . Afterwards, the cells were stimulated with ligands which increasing concentrations for at least  $5 \text{ min}$  at room temperature. Ligands were diluted from  $1 \text{ nM}$  to  $1\text{mM}$  in PBS buffer. By a Multimode Plate Reader (PerkinElmer EnVision), luminescence per well per second (LCPS) was read. Using the sigmoidal dose–response function which was in GraphPad Prism 8.0 analyzed Data.

### **Ligand bias assay**

Bioluminescence resonance energy transfer (BRET) assay was performed as previously described (13, 14). Flag-GPBAR-eYFP,  $\beta$ -arrestin 1-Rluc plasmids were co-transfected into HEK-293 cells using Lipofectamine™ 2000 (Thermo Fisher) at  $37^\circ\text{C}$  with  $5\% \text{ CO}_2$  for  $24 \text{ h}$ . And then the transfected cells were seeded in white  $96$ -well plates at  $40000$  cells per well and cultured in  $37 \text{ }^\circ\text{C}$  incubator for another  $24 \text{ h}$ . Before

the BRET assay, the cells were washed three times with PBS, and treated with R399/INT-777/LCA for 2 minutes. The Luciferase Substrate Coelenterazine h (work concentration: 5 $\mu$ M) was added to the white 96-well plates. Data were read in the Mithras LB940 microplate reader (Berthold Technologies), which was equipped with 530 nm and 485 nm emissions. The BRET signal was represented by calculating the ratio of the light emitted by eYFP and the light emitted by Rluc.

$$\beta = \log \left( \left[ \frac{E_{\max,P1}}{EC_{50,P1}} \frac{EC_{50,P2}}{E_{\max,P2}} \right]_{\text{lig}} \times \left[ \frac{E_{\max,P2}}{EC_{50,P2}} \frac{EC_{50,P1}}{E_{\max,P1}} \right]_{\text{ref}} \right)$$

P1: cAMP data, P2: BRET data,  $\beta > 0$ , Gs biased;  $\beta < 0$ , Arrestin biased

### Statistical analysis

Every experiment was independently repeated at least in triplicate. All data were expressed as the mean and standard deviation (Mean  $\pm$  SEM). Statistical analysis was performed using GraphPad Prism8.0 (Graph Pad Software, San Diego, CA, USA). Differences between groups were evaluated with two-tailed Student's t-test.  $P < 0.05$  was considered statistically significant. The cryo-EM density map for R399-GPBAR-Gs complex has been deposited in the Electron Microscopy Data Bank (EMDB) under accession codes EMD-33452. The coordinate for the model of R399-GPBAR-Gs has been deposited in the PDB under accession number 7XTQ.

### REFERENCES

1. Yin C, *et al.* (2020) FAM83D promotes epithelial-mesenchymal transition, invasion and cisplatin resistance through regulating the AKT/mTOR pathway in non-small-cell lung cancer. *Cell Oncol (Dordr)* 43(3):395-407.
2. Liang YL, *et al.* (2018) Phase-plate cryo-EM structure of a biased agonist-bound human GLP-1 receptor-Gs complex. *Nature* 555(7694):121-125.
3. Cleator JH, Mehta ND, Kurtz DT, & Hildebrandt JD (1999) The N54 mutant of Galphas has a conditional dominant negative phenotype which suppresses hormone-stimulated but not basal cAMP levels. *FEBS Lett* 443(2):205-208.
4. Iiri T, Bell SM, Baranski TJ, Fujita T, & Bourne HR (1999) A Gsalpha mutant designed to inhibit receptor signaling through Gs. *Proc Natl Acad Sci U S A* 96(2):499-504.
5. Lee E, Taussig R, & Gilman AG (1992) The G226A mutant of Gs alpha highlights the requirement for dissociation of G protein subunits. *J Biol Chem* 267(2):1212-1218.
6. Xu YF, *et al.* (2021) PTP-MEG2 regulates quantal size and fusion pore opening through two distinct structural bases and substrates. *EMBO Rep* 22(5):e52141.

7. Wang Y, *et al.* (2017) Distinct Interactions of EBP1 Isoforms with FBXW7 Elicits Different Functions in Cancer. *Cancer Res* 77(8):1983-1996.
8. Zhan P, *et al.* (2017) alpha-enolase promotes tumorigenesis and metastasis via regulating AMPK/mTOR pathway in colorectal cancer. *Mol Carcinog* 56(5):1427-1437.
9. Olsen RHJ, *et al.* (2020) TRUPATH, an open-source biosensor platform for interrogating the GPCR transducerome. *Nat Chem Biol* 16(8):841-849.
10. Yang F, *et al.* (2021) Structure, function and pharmacology of human itch receptor complexes. *Nature* 600(7887):164-169.
11. Fan F, *et al.* (2008) Novel genetically encoded biosensors using firefly luciferase. *ACS Chem Biol* 3(6):346-351.
12. Hu QX, *et al.* (2014) Constitutive Galphai coupling activity of very large G protein-coupled receptor 1 (VLGR1) and its regulation by PDZD7 protein. *J Biol Chem* 289(35):24215-24225.
13. Rajagopal S, *et al.* (2011) Quantifying ligand bias at seven-transmembrane receptors. *Molecular pharmacology* 80(3):367-377.
14. Yang F, *et al.* (2018) Allosteric mechanisms underlie GPCR signaling to SH3-domain proteins through arrestin. *Nat Chem Biol* 14(9):876-886.